Motion planning and posture control of multiple *n*-link doubly nonholonomic manipulators

Bibhya Sharma, Jito Vanualailai and Shonal Singh

Robotica / *FirstView* Article / April 2015, pp 1 - 25
DOI: 10.1017/S0263574714002604, Published online: 05 March 2015

Link to this article: http://journals.cambridge.org/abstract_S0263574714002604

How to cite this article:
Bibhya Sharma, Jito Vanualailai and Shonal Singh Motion planning and posture control of multiple *n*-link doubly nonholonomic manipulators. Robotica, Available on CJO 2015 doi:10.1017/S0263574714002604

Robotica: page 1 of 25.
doi:10.1017/S0263574714002604

Motion planning and posture control of multiple *n*-link doubly nonholonomic manipulators

Bibhya Sharma*, Jito Vanualailai and Shonal Singh

The University of the South Pacific, FIJI

(Accepted October 16, 2014)

SUMMARY

The paper considers the problem of motion planning and posture control of multiple n-link doubly nonholonomic mobile manipulators in an obstacle-cluttered and bounded workspace. The workspace is constrained with the existence of an arbitrary number of fixed obstacles (disks, rods and curves), artificial obstacles and moving obstacles. The coordination of multiple n-link doubly nonholonomic mobile manipulators subjected to such constraints becomes therefore a challenging navigational and steering problem that few papers have considered in the past. Our approach to developing the controllers, which are novel decentralized nonlinear acceleration controllers, is based on a Lyapunov control scheme that is not only intuitively understandable but also allows simple but rigorous development of the controllers. Via the scheme, we showed that the avoidance of all types of obstacles was possible, that the manipulators could reach a neighborhood of their goal and that their final orientation approximated the desired orientation. Computer simulations illustrate these results.

KEYWORDS: Lyapunov-based control scheme; Doubly nonholonomic manipulators; Ghost parking bays; Minimum distance technique; Stability; Kinodynamic constraints.

1. Introduction

1.1. Motivational work

In the last two decades, roboticists have considered various types of navigation schemes that allow multiple agents to achieve common or shared goals. Rules and behavioral patterns from nature have been mimicked, modelled and applied to solve real-life applications. The applications include dull, dirty, dangerous and difficult tasks such as surveillance, construction, transportation and traffic control, health care, mining and sampling, reconnaissance, mowing, museum guides and space exploration.[1–6] The tasks can be performed in environments which may even be inaccessible to humans[7] or could involve repetitions.

The use of multiple agents as opposed to single agents holds practical and theoretical advantages in various contexts and situations. These, *inter alia*, include desired functionalities with stringent time and cost constraints, increased robustness, greater fault tolerance, better safety, accelerated performance and enhanced capabilities.[1,4,7] The advantages are clearly due to the cooperation and networking capabilities between agents, parallel processing power capability presented by several agents, or simply due to an increased presence in the environment. However, physical limitations, possible interference and computational problems such as role and task allocations may surface in certain situations.[1,8] Notwithstanding these drawbacks, the advantages outweigh the disadvantages; hence researchers are continuously developing and designing efficient task or behavior-based algorithms for multiple robotic agents under various conditions.

Mobile manipulators have been considered to tackle complicated problems such as the one described in this paper because of their mobility, which can classified into four types:[4,9–13] (1) Type (h, h), where both platform and manipulator contain holonomic constraints; (2) Type (h, nh),

* Corresponding author. E-mail: sharma_b@usp.ac.fj

where the platform is holonomic and the manipulator is nonholonomic; (3) Type (nh, h), where the platform is nonholonomic but the manipulator is holonomic; and (4) Type (nh, nh), where both the platform and the manipulator contain nonholonomic constraints.

In this paper, we consider type (nh, nh) mobile manipulators which were introduced by Tchoń *et al.* in[14] 2004 and classified as the *doubly nonholonomic mobile manipulators*. A review of the literature on motion planning and control of type (nh, nh) mobile manipulators reveals a relatively recent activity carried out by only a handful of researchers. Tchoń *et al.* presented the kinematics theory of type (nh, nh), which is composed of a mobile nonholonomic wheeled platform equipped with a planar n-link nonholonomic manipulator. Such a system is able to autonomously perform manipulation of tasks in environments where more configurations are reachable than compared to those by anchored manipulators.[12] Challenges one may face in autonomously controlling the motion of type (nh, nh) mobile manipulators are the complexity of the control algorithms, intensive computations and the difficulty of simulations, given the intimate coupling of the double nonholonomic constraints arising from the union of an articulated robotic arm and a wheeled platform. These challenges motivate the authors to develop an effective control scheme for such manipulators.

1.2. Background on collision avoidance schemes

The literature harbors a variety of algorithms addressing the motion planning and control of mobile robots. They include the artificial potential field methods, graph search techniques, road maps and neural network models.[15–19] While the algorithms generated from graph search techniques and road maps are elegant, they are computationally intensive and at times suffer from the problem of *too close*.[20] The neural network models, although robust are predominantly based on learning and estimations.[16,21]

The pioneer work on motion planning and control of robots via artificial potential fields was carried out by Khatib in[22] and this was followed by an abundance of work within the framework.[4,5,23–27] The governing principle behind the method is to attach an attractive field to the target and a repulsive field to each obstacle. The workspace is inundated with positive and negative fields, with the direction of motion facilitated via the notion of steepest descent.[22] The method is favored due to an easier analytic representation of system singularities and inequalities, increased processing speed and its simplicity and elegance, although it inherently involves the problem of *local minima*. In this paper, we have adopted an artificial potential field method known as the Lyapunov-based control scheme (LbCS) from.[5] The scheme has been recently applied to motion planning and control of various robotic systems, including ones tagged with holonomic or nonholonomic constraints.[4,26,28] The seminal idea behind this control scheme is to design the attractive and repulsive potential functions which are summed to form a suitable Lyapunov function that acts as an artificial potential field function or *total potentials*. From this, the nonlinear controllers, centralized or decentralized, velocity or acceleration-based, are extracted. The advantage of the method remains with the simplicity in designing the controllers.

In 2012, the authors first showed that the LbCS is well-suited for type (nh, nh) mobile manipulators.[28] The authors applied the method to a single type (nh, nh) mobile manipulator and showed the effectiveness of the method in developing controllers for navigating the manipulator among rod-shaped, disk-shaped and polygonal obstacles. This paper extends the 2012 results in a very comprehensive manner by considering multiple type (nh, nh) mobile manipulators moving in a similarly cluttered workspace.

1.3. Contributions

A type (nh, nh) mobile manipulator is normally composed of a mobile nonholonomic wheeled platform equipped with a planar n-link nonholonomic manipulator. The challenges of the type (nh, nh) design are the complexity of the control algorithms, intensive computations and the difficulty of simulations, given the intimate coupling of the double nonholonomic constraints arising from the union of an articulated robotic arm and a wheeled platform. It is mainly because of this reason that only a small number of researchers consider type (nh, nh) manipulators for complex tasks.[11,12,14,28]

While the control strategies of mobile manipulators can either be centralized such as in[9,10] or decentralized such as in,[11–13] to the best of the authors' knowledge, there is no decentralized acceleration control laws that solve the motion planning and posture control problem of multiple type (nh, nh) manipulators.

In this paper, the authors deploy the Lyapunov-based control scheme to provide a simple but effective means of harnessing decentralized control laws of multiple n-link doubly nonholonomic mobile manipulators, hereafter, denoted as nDNMs. The framework also offers an extended degree of flexibility by taking into account the final configurations and all the constraints pertaining to the robotic system which includes, *inter alia*, limitations on velocity and steering angle, singular configurations of the manipulator system, restrictions imposed by workspace and obstacles (moving, stationary and artificial) in the workspace.

1.4. Organization

This paper is organized as follows: in Section 2 the doubly nonholonomic mobile manipulator robot model is defined; in Section 3 we state the control objective; in Section 4 we provide a brief overview of the Lyapunov-based control scheme (LbCS); in Section 5 the artificial potential field functions are created in accordance with the LbCS; in Section 6 the decentralized acceleration controllers are designed and stability analysis of the n-link mobile manipulators carried out; in Section 7 computer simulations of two scenarios are carried out; and Section 8 concludes the paper and outlines future work in the area.

2. Vehicle Model

Definition 1. *Let $\mathcal{A}_i$, $i \in \{1, 2, \ldots, N\}$, $N \in \mathbb{N}$, represent the ith n-link doubly nonholonomic mobile manipulator, written in short-hand notation as the ith nDNM. It consists of a nonholonomic car-like wheeled platform with a n-link nonholonomic manipulator mounted on the mid-front axle of the platform. For each $\mathcal{A}_i$, the wheeled platform is a disk with radius r_0 and is positioned at the center (x_{i0}, y_{i0}). Precisely, the wheeled platform is the set*

$$\mathcal{P}_i := \left\{(z_1, z_2) \in \mathbb{R}^2 : (z_1 - x_{i0})^2 + (z_2 - y_{i0})^2 \leq r_0^2\right\}.$$

Link k, $k = 1, 2, \ldots, n$, is a disk centered at (x_{ik}, y_{ik}) with radius r_k. Link k of $\mathcal{A}_i$ can thus be defined as

$$\mathcal{L}_{ik} := \left\{(z_1, z_2) \in \mathbb{R}^2 : (z_1 - x_{ik})^2 + (z_2 - y_{ik})^2 \leq r_k^2\right\}.$$

Precisely, the ith nDNM is described by the set

$$\mathcal{A}_i := \{(z_1, z_2) \in \mathbb{R}^2 : \mathcal{P}_i \cup \mathcal{L}_{i1} \cup \mathcal{L}_{i2} \cup \cdots \cup \mathcal{L}_{in}\}.$$

As an illustration of Definition 2, we provide the schematics of a 4-link doubly nonholonomic mobile manipulator in the inertial frame $\mathcal{F}$, see Fig. 1. The inertial frame $\mathcal{F}$ is the Cartesian coordinate z_1-z_2 plane as shown in Fig. 1. We adopt the novel approach presented by Nakamura *et al.*[29] in designing the n-link nonholonomic manipulator. The approach encompasses the design of a new nonholonomic mechanical gear which is able to transmit velocities to many passive joints. The nonholonomic constraints in the gear appear by assumption on rolling contact without slippage between balls of a gear and special supporting wheels in the robot joints. The reader is referred to Mazur and Szakiel in[12] for a detailed overview of the nonholonomic manipulator. We assume no slippage (i.e., $\dot{x}_{i0} \sin\theta_{i0} - \dot{y}_{i0} \cos\theta_{i0} = 0$) and pure rolling (i.e., $\dot{x}_{i0} \cos\theta_{i0} + \dot{y}_{i0} \sin\theta_{i0} = v_i$) of the car-like mobile platform of the ith nDNM.

Now, with reference to Fig. 1, the (x_i, y_i) coordinates give the position of the end-effector, ϕ_i gives the platform's steering angle with respect to its longitudinal axis, while ℓ_0 and b_0 are, respectively, the length and width of the platform. Furthermore, ℓ_k is the length of Link k, $k \in \{1, 2, \ldots, n\}$. The reader is referred to Table I for a list of variables that will be used to describe the dynamic model of each $\mathcal{A}_i$.

In Sharma *et al.*,[28] we have derived in detail the dynamic model of a single nDNM. Thus, the dynamic model of $\mathcal{A}_i$, $i \in \{1, 2, \ldots, N\}$, with respect to the position of its end-effector $(x_i, y_i) \in \mathbb{R}^2$

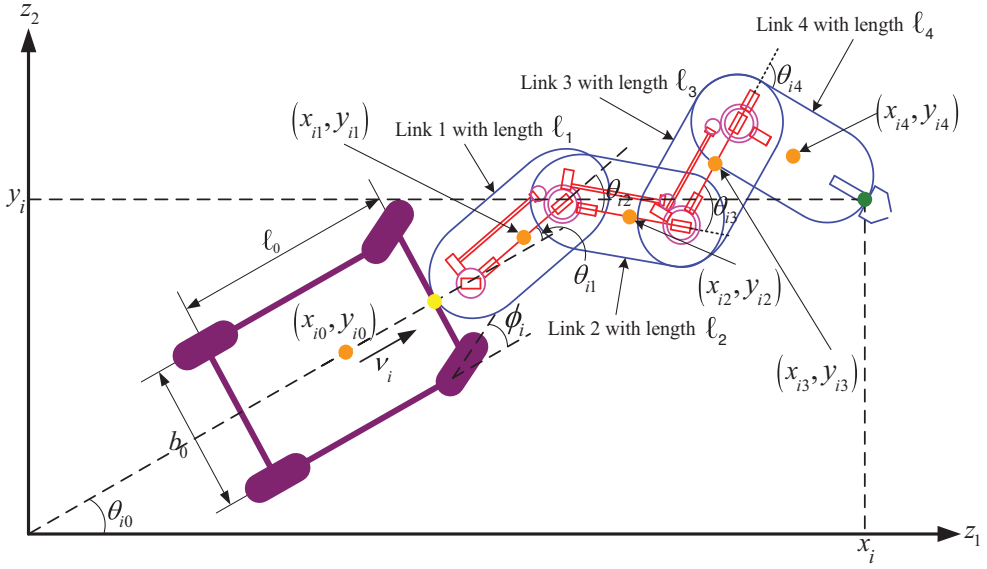

Fig. 1. (Colour online) Illustration of the ith 4DNM in the inertial frame $\mathcal{F}$. The schematics of the 4-link nonholonomic manipulator is adopted from.[29]

defined in the inertial frame $\mathcal{F}$ is given as

$$
\left.
\begin{aligned}
\dot{x}_i &= v_i \cos\theta_{i0} - \ell_0 \omega_{i0} \sin\theta_{i0} - \left[\sum_{k=1}^{n} \ell_k \sin\left(\sum_{p=0}^{k} \theta_{ip}\right)\right](\omega_{i0} + \omega_{i1}) \\
&\quad - \left\{\sum_{k=2}^{n} \ell_k \left[\sum_{p=2}^{k} \left(a_{ip} \sin\theta_{i\,p-1} \prod_{j=1}^{p-2} \cos\theta_{ij}\right) \sin\left(\sum_{p=0}^{k} \theta_{ip}\right)\right]\right\} \omega_{i2}, \\
\dot{y}_i &= v_i \sin\theta_{i0} + \ell_0 \omega_{i0} \cos\theta_{i0} + \left[\sum_{k=1}^{n} \ell_k \cos\left(\sum_{p=0}^{k} \theta_{ip}\right)\right](\omega_{i0} + \omega_{i1}) \\
&\quad + \left\{\sum_{k=2}^{n} \ell_k \left[\sum_{p=2}^{k} \left(a_{ip} \sin\theta_{i\,p-1} \prod_{j=1}^{p-2} \cos\theta_{ij}\right) \cos\left(\sum_{p=0}^{k} \theta_{ip}\right)\right]\right\} \omega_{i2}, \\
\dot{\theta}_{i0} &= \omega_{i0}, \qquad \dot{\theta}_{i1} = \omega_{i1}, \\
\dot{\theta}_{ik} &= \left(a_{ik} \sin\theta_{i\,k-1} \prod_{j=1}^{k-2} \cos\theta_{ij}\right) \omega_{i2}, \quad k = 2, 3, \ldots, n, \\
\dot{v}_i &= u_{i1}, \qquad \dot{\omega}_{i0} = u_{i2}, \qquad \dot{\omega}_{i1} = u_{i3}, \qquad \dot{\omega}_{i2} = u_{i4},
\end{aligned}
\right\} \tag{1}
$$

where a_{ik} are positive coefficients, depending on gear ratios. Note that $\prod_{j=1}^{k-2} \cos\theta_{ij} = 1$ whenever $k - 2 < j$. Also, we note that all the nonholonomic constraints are already factored into the ODEs governing system (1).

Now, system (1) is a description of the instantaneous velocities and accelerations of the various components of $\mathcal{A}_i$. Let the vector $\mathbf{x}_i := (x_i, y_i, \theta_{i0}, \theta_{i1}, \theta_{i2}, \ldots, \theta_{in}, v_i, \omega_{i0}, \omega_{i1}, \omega_{i2}) \in \mathbb{R}^{n+7}$ refer to the position (x_i, y_i) of the end-effector of $\mathcal{A}_i$, the orientations $(\theta_{i0}, \theta_{i1}, \theta_{i2}, \ldots, \theta_{in})$ of the various components of $\mathcal{A}_i$ and the velocities $(v_i, \omega_{i0}, \omega_{i1}, \omega_{i2})$ of the various components of $\mathcal{A}_i$ at time $t \geq 0$.

Table I. Description of the system variables in the dynamic model of each $\mathcal{A}_i$, $i \in \{1, 2, \ldots, N\}$.

Variable	Description
$x_{i0}(t)$	z_1-component of the position of the center of the platform
$y_{i0}(t)$	z_2-component of the position of the center of the platform
$x_{ik}(t)$	z_1-component of the position of the center of Link k, $k \in \{1, 2, \ldots, n\}$
$y_{ik}(t)$	z_2-component of the position of the center of Link k, $k \in \{1, 2, \ldots, n\}$
$\theta_{i0}(t)$	Angular position of platform with respect to the z_1-axis
$\theta_{i1}(t)$	Angular position of Link 1 with respect to the platform
$\theta_{ik}(t)$	Angular position of Link k with respect to Link $k-1$, $k = 2, 3, \ldots, n$
$v_i(t)$	Linear velocity of the wheels of the platform
$\omega_{i0}(t)$	Angular velocity of the platform
$\omega_{i1}(t)$	Angular velocity of joint 1 (active joint) of the manipulator
$\omega_{i2}(t)$	Angular velocity of the driving input wheel located at joint 1
$u_{i1}(t)$	Linear acceleration of the wheels of the platform
$u_{i2}(t)$	Angular acceleration of the platform
$u_{i3}(t)$	Angular acceleration of joint 1
$u_{i4}(t)$	Angular acceleration of the driving input wheel located at joint 1

Now, let

$$\begin{aligned}\mathbf{f}_i(\mathbf{x}_i) &= (f_{i1}(\mathbf{x}_i), f_{i2}(\mathbf{x}_i), g_{i1}(\mathbf{x}_i), \ldots, g_{i\,n+1}(\mathbf{x}_i), 0, 0, 0, 0)\\ &:= \left(\dot{x}_i, \dot{y}_i, \dot{\theta}_{i0}, \ldots, \dot{\theta}_{in}, 0, 0, 0, 0\right) \in \mathbb{R}^{n+7},\end{aligned}$$

and $\mathbf{u}_i(t) := (u_{i1}(t), u_{i2}(t), u_{i3}(t), u_{i4}(t)) \in \mathbb{R}^4$. Then system (1) can be written compactly as

$$\dot{\mathbf{x}}_i := \mathbf{f}_i(\mathbf{x}_i) + \mathbf{B}_i\mathbf{u}_i(t), \tag{2}$$

where $\mathbf{B}_i$ is a $(n+7) \times 4$ matrix of the form

$$\mathbf{B}_i = \begin{bmatrix} 0\,0\,0\,0 \\ 0\,0\,0\,0 \\ 0\,0\,0\,0 \\ \vdots\,\vdots\,\vdots\,\vdots \\ 1\,0\,0\,0 \\ 0\,1\,0\,0 \\ 0\,0\,1\,0 \\ 0\,0\,0\,1 \end{bmatrix}.$$

Let $\mathbf{x} := (\mathbf{x}_1, \mathbf{x}_2, \ldots, \mathbf{x}_N) \in \mathbb{R}^{(n+7)\times N}$ refer to the positions, orientations and the velocities of all the N nDNMs. Let $\mathbf{f}(\mathbf{x}) := (\mathbf{f}_1(\mathbf{x}), \mathbf{f}_2(\mathbf{x}), \ldots, \mathbf{f}_N(\mathbf{x})) \in \mathbb{R}^{(n+7)\times N}$ and $\mathbf{u}(t) := (\mathbf{u}_1(t), \mathbf{u}_2(t), \cdots, \mathbf{u}_N(t)) \in \mathbb{R}^{4N}$. Then we have the following initial-value problem for N nDNMs:

$$\dot{\mathbf{x}} = \mathbf{f}(\mathbf{x}) + \mathbf{B}\mathbf{u}(t), \quad \mathbf{x}(t_0) =: \mathbf{x}_0, \quad t_0 \geq 0, \tag{3}$$

where, if $\mathbf{0}$ is a $(n+7) \times 4$ matrix of all zero entries,

$$\mathbf{B} = \begin{bmatrix} \mathbf{B}_1 & \mathbf{0} & \cdots & \mathbf{0} \\ \mathbf{0} & \mathbf{B}_2 & \cdots & \mathbf{0} \\ \vdots & \vdots & \ddots & \vdots \\ \mathbf{0} & \mathbf{0} & \cdots & \mathbf{B}_N \end{bmatrix}.$$

Now, assume that the final position of the end-effector of $\mathcal{A}_i$ is at the point $(x_i, y_i) = (p_{i1}, p_{i2})$ and final orientation at this point is $(\theta_{i0}, \theta_{i1}, \ldots, \theta_{in}) = (p_{i3}, p_{i4}, \ldots, p_{i\,n+3})$. Its final instantaneous

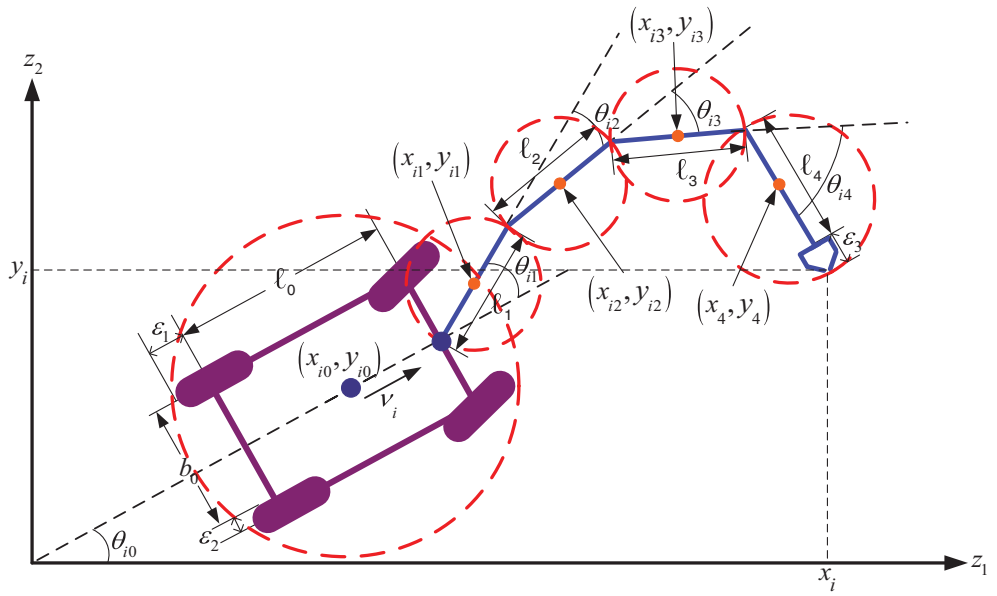

Fig. 2. (Colour online) The protective regions of the ith 4DNM.

velocity vector is $(v_i, \omega_{i0}, \omega_{i1}, \omega_{i2}) = (0, 0, 0, 0)$. Then it is clear that the points

$$\mathbf{x}_i^* := (p_{i1}, p_{i2}, p_{i3}, p_{i4}, \ldots, p_{i\,n+3}, 0, 0, 0, 0) \in \mathbb{R}^{n+7}$$

are the components of the equilibrium point of system (3) in which we are interested, that is,

$$\mathbf{x}^* := (\mathbf{x}_1^*, \mathbf{x}_2^*, \ldots, \mathbf{x}_N^*) \in \mathbb{R}^{(n+7)\times N}.$$

Now, to ensure that the entire body of $\mathcal{A}_i$ safely steers past an obstacle, we enclose each body of $\mathcal{A}_i$ by the smallest protective region possible (see Fig. 2). Precisely, given the *clearance parameters* $\varepsilon_1 > 0$ and $\varepsilon_2 > 0$, a circular protective region centered at (x_{i0}, y_{i0}) with radius $r_0 = \sqrt{(\ell_0 + 2\varepsilon_1)^2 + (b_0 + 2\varepsilon_2)^2}/2$ can be considered for the mobile platform, in this case, a car-like robot. For Link k ($k = 1, 2, \ldots, n-1$), we use circular protective regions centered at (x_{ik}, y_{ik}) with radius $r_k = \ell_k/2$. For Link n, we use a circular protective region centered at (x_{in}, y_{in}) with radius $r_n = \ell_n/2 + \varepsilon_3$ (where $\varepsilon_3 > 0$ is the *safety parameter* needed to protect the gripper).

Also, it can easily be verified that we can express the positions of the mobile car-like platform and Link k of $\mathcal{A}_i$ completely in terms of the state variables x_i, y_i, θ_{i0} and θ_{ik}. For example, for the n links of $\mathcal{A}_i$, we have

$$x_{im} = x_i - \sum_{k=m}^{n} \frac{\ell_k}{2^{\lfloor \frac{m+1}{k+1} \rfloor}} \cos\left(\sum_{p=0}^{k} \theta_{ip}\right),$$
$$y_{im} = y_i - \sum_{k=m}^{n} \frac{\ell_k}{2^{\lfloor \frac{m+1}{k+1} \rfloor}} \sin\left(\sum_{p=0}^{k} \theta_{ip}\right),$$

which gives the Cartesian position (x_{im}, y_{im}) of the center of the mth link, $m = 1, 2, \ldots, n$, in the inertial frame $\mathcal{F}$. Since these are positional measures only they do not include the nonholonomic constraints. Therefore, the equations are exactly the same as the type (nh, h) ones, where the platform is nonholonomic but the manipulator is holonomic (see for example[4]).

3. Control Objective

Our objective is to design the acceleration controllers u_{i1}, u_{i2}, u_{i3}, and u_{i4}, for $\mathcal{A}_i$, $i \in \{1, 2, \ldots, N\}$, such that they autonomously and safely coordinate multiple nDNMs in a decentralized manner, navigate the manipulators successfully past obstacles in the workspace, guide them to a neighborhood of their designated targets and align each manipulator in a final orientation that approximates its predefined final orientation.

4. An Overview of a Lyapunov-based Control Scheme

To design the controllers, we shall use a Lyapunov-based control scheme (LbCS) proposed in.[5] According to the control scheme, we construct attractive and obstacle avoidance functions for the attraction to targets and repulsion from various obstacles, respectively. We note that these functions are basically Euclidean measures between the robots and the targets, or obstacles. The sum of these potential functions is termed as the *total potentials*. As an overview of the scheme's application, consider a point-mass moving in a rectangular workspace since the exposition leads smoothly to the development of the controllers of the mobile manipulators. The point-mass is required to move to its target while avoiding a stationary object in the workspace.

Definition 2. *The point-mass $\mathcal{P}_M$ is a disk of radius $r_P \geq 0$ and is positioned at $(x(t), y(t)) \in \mathbb{R}^2$ at time $t \geq 0$. Precisely, the point-mass is the set*

$$\mathcal{P}_M := \left\{(z_1, z_2) \in \mathbb{R}^2 : (z_1 - x)^2 + (z_2 - y)^2 \leq r_P^2\right\},$$

with respect to the z_1-z_2 plane.

Definition 3. *The designated target for the point-mass $\mathcal{P}_M$ is a disk with center (p_1, p_2) and radius $r_T > 0$. That is, it is the set*

$$T := \{(z_1, z_2) \in \mathbb{R}^2 : (z_1 - p_1)^2 + (z_2 - p_2)^2 \leq r_T^2\}.$$

Definition 4. *The stationary solid object is a circular disk with center (o_1, o_2) and radius $r_O > 0$. Precisely, the solid object is the set*

$$O := \{(z_1, z_2) \in \mathbb{R}^2 : (z_1 - o_1)^2 + (z_2 - o_2)^2 \leq r_O^2\}.$$

For target attraction, we require a measurement of the Euclidean distance between the position (x, y) of the point-mass $\mathcal{P}_M$ and its target T. Therefore, a likely attractive potential function is

$$H(x, y) := \frac{1}{2}\left[(x - p_1)^2 + (y - p_2)^2\right].$$

For obstacle avoidance, we require a measurement of the Euclidean distance between the centers of the point-mass $\mathcal{P}_M$ and the obstacle O. Thus, a likely potential function is

$$FO(x, y) := \frac{1}{2}\left[(x - o_1)^2 + (y - o_2)^2 - (r_P + r_O)^2\right].$$

Given a scalar $\alpha > 0$ (a *tuning* or *control parameter*), the total potential field that can guarantee target convergence and obstacle avoidance is defined as the sum of the attractive and repulsive potential fields, and is generated by the total potential field function

$$H(x, y) + \frac{\alpha}{FO(x, y)}. \tag{4}$$

In Fig. 3, as an illustration, we show the total potential field generated by Eq. (4) to guide the point-mass $\mathcal{P}_M$ to a target placed at (20, 20) – the minimum of the field.

Using the same approach, we develop a total potential function for the multiple manipulators and use it to derive the acceleration controllers for each $\mathcal{A}_i$.

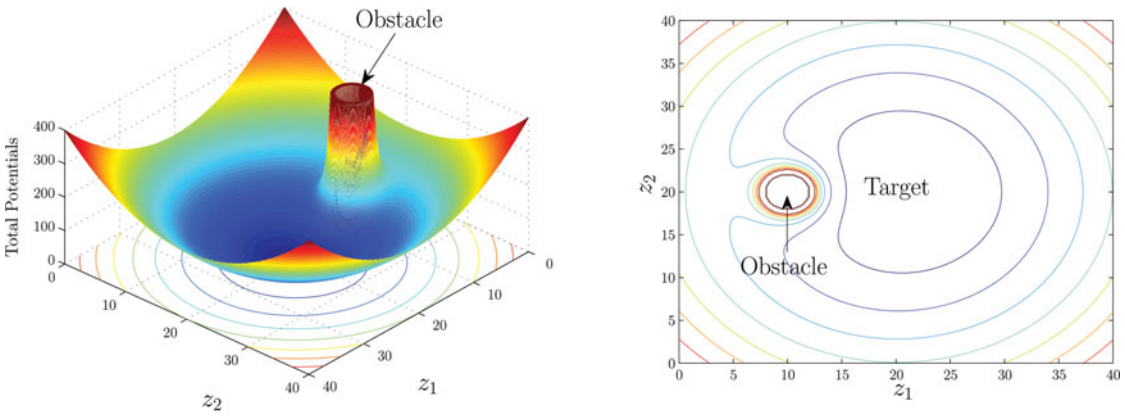

(a) 3D Visualization (b) Contour Plot

Fig. 3. (Colour online) The total potentials generated by Eq. (4). The target is located at $(p_1, p_2) = (20, 20)$ with radius $r_T = r_P = 1$ and the obstacle is fixed at $(o_1, o_2) = (10, 20)$ with a radius of $r_O = 2$. The value of the tuning parameter is chosen as $\alpha = 10$. (a) 3D Visualization. (b) Contour plot.

5. Attraction and Avoidance Functions

It is assumed that for each $\mathcal{A}_i$, the final postures (final position of the end-effector and final orientations of each component of $\mathcal{A}_i$ at the target) are predefined. It is also assumed, unless otherwise stated, that for all the target attraction and obstacle avoidance functions that will be derived in this section, we have $i \in \{1, 2, \ldots, N\}$ for $\mathcal{A}_i$, and $m \in \{0, 1, \ldots, n\}$, for the mth articulated body of $\mathcal{A}_i$ for $n \geq 3$ and $n, N \in \mathbb{N}$. We note that for each $\mathcal{A}_i$, if $n = 1$, the manipulator is over-actuated. If $n = 2$, the manipulator is fully-actuated. The interesting cases involve under-actuated n-link doubly nonholonomic manipulator systems that arise when $n \geq 3$. Hence, the above assumption that $n \geq 3$ for the ith nDNM.

5.1. Functions for target attraction and final orientation

For the end-effector of $\mathcal{A}_i$, we assign a circular target with center (p_{i1}, p_{i2}) and radius $rt_i > 0$. We define the target as

$$T_i := \{(z_1, z_2) \in \mathbb{R}^2 : (z_1 - p_{i1})^2 + (z_2 - p_{i2})^2 \leq rt_i^2\}.$$

For its attraction, we consider the target attractive function

$$H_i(\mathbf{x}) := \frac{1}{2}\left[(x_i - p_{i1})^2 + (y_i - p_{i2})^2 + v_i^2 + \sum_{j=0}^{2} \omega_{ij}^2\right], \tag{5}$$

which is nonnegative for all $\mathbf{x} \in \mathbb{R}^{(n+7)\times N}$.

On orientation, we adopt the concepts of the minimum distance technique (MDT) and the ghost parking bays from Sharma *et al.*[5] to achieve the final orientation of the wheeled platform of $\mathcal{A}_i$. There is one ghost parking bay for each $\mathcal{A}_i$. Each parking bay consists of three ghost walls making up a rectangular shape, with an open end for entry. To achieve the final orientations, these ghost walls have to be avoided.

To avoid the ghost walls, we use the MDT to identify the closest point on each Kth ghost wall measured from the reference point of the platform of $\mathcal{A}_i$. Avoidance of these closest points on a ghost wall at any time $t \geq 0$ essentially results in the avoidance of the entire wall by the platform of $\mathcal{A}_i$.

Now, given the *saturation function* $\Lambda_{iK} : \mathbb{R}^2 \to [0, 1] \subset \mathbb{R}$, defined as

$$\Lambda_{iK}(x_{i0}, y_{i0}) := \begin{cases} 0 & , \text{if } \Lambda_{iK} < 0, \\ \Lambda_{iK} & , \text{if } 0 \leq \Lambda_{iK} \leq 1, \\ 1 & , \text{if } \Lambda_{iK} > 1, \end{cases}$$

we can obtain the parametric representation of this Kth ghost wall in the z_1-z_2 plane with initial coordinates (A_{K1}, B_{K1}) and final coordinates (A_{K2}, B_{K2}) as

$$C_{iK} := A_{K1} + \Lambda_{iK}(A_{K2} - A_{K1}), \qquad D_{iK} := B_{K1} + \Lambda_{iK}(B_{K2} - B_{K1}).$$

Minimizing the Euclidean distance between the point (x_{i0}, y_{i0}) and the ghost wall (C_{iK}, D_{iK}), we get

$$\Lambda_{iK} = (x_{i0} - A_{K1})Q_{K1} + (y_{i0} - B_{K1})Q_{K2}, \quad \text{for} \quad \Lambda_{iK} \in [0, 1],$$

where

$$Q_{K1} := \frac{A_{K2} - A_{K1}}{(A_{K2} - A_{K1})^2 + (B_{K2} - B_{K1})^2} \qquad \text{and} \qquad Q_{K2} := \frac{B_{K2} - B_{K1}}{(A_{K2} - A_{K1})^2 + (B_{K2} - B_{K1})^2}.$$

We note that $\Lambda_{iK}(x_{i0}, y_{i0})$ is a nonnegative scalar such that it is restricted to the interval [0,1]. As a result there is always an avoidance of the Kth ghost wall at every time $t \geq 0$.

Each target will be surrounded by three ghost walls, which have to be avoided by the platform of the respective $\mathcal{A}_i$. This means that the platform of the ith nDNM will be avoiding $(3i - 2)$st, $(3i - 1)$nd and $(3i)$rd ghost walls; thus $K \in \{3i - 2, 3i - 1, 3i\}$. The following obstacle avoidance function will ensure that the platform of $\mathcal{A}_i$ will avoid the time-varying closest points on the ghost walls positioned at the target configuration of the ith robot:

$$PB_{iK}(\mathbf{x}) := \frac{1}{2}\left[(x_{i0} - C_{iK})^2 + (y_{i0} - D_{iK})^2 - r_0^2\right],$$

for $K \in \{3i - 2, 3i - 1, 3i\}$.

Given some (*tuning* or *control*) parameter $\tau_{iK} > 0$, we can form the repulsive potential field function

$$\sum_{i=1}^{N} \sum_{K=3i-2}^{3i} \frac{\tau_{iK}}{PB_{iK}(\mathbf{x})}.$$

Consider, for example, the presence of one 3DNM (that is, $N = 1$ and $n = 3$). The total potential field that governs the motion of the 3DNM, denoted as $\mathcal{A}_1$, is

$$H_1(\mathbf{x}) + \sum_{K=1}^{3} \frac{\tau_{1K}}{PB_{1K}(\mathbf{x})}. \tag{6}$$

Figure 4 presents a 3D view of the total potential field and the corresponding contour plot produced by Eq. (6).

5.2. Functions for obstacle avoidance

In this section we list all different types of obstacles and propose functions for their avoidance. Some of these obstacles are physical obstacles residing within the workspace, which is defined below:

Definition 5. *The planar workspace is a fixed, closed and bounded rectangular region defined for some* $\eta_1 > 2\sum_{m=0}^{n} r_m$ and $\eta_2 > 2\sum_{m=0}^{n} r_m$ as the set

$$WS := \{(z_1, z_2) \in \mathbb{R}^2 : 0 \leq z_1 \leq \eta_1, 0 \leq z_2 \leq \eta_2\}.$$

5.2.1. Workspace boundaries as obstacles. We begin by noting that the left, lower, right, and upper boundaries of the workspace can be defined as follows:

$$B_1 := \{(z_1, z_2) \in \mathbb{R}^2 : z_1 = 0\}, \qquad B_2 := \{(z_1, z_2) \in \mathbb{R}^2 : z_2 = 0\},$$
$$B_3 := \{(z_1, z_2) \in \mathbb{R}^2 : z_1 = \eta_1\}, \qquad B_4 := \{(z_1, z_2) \in \mathbb{R}^2 : z_2 = \eta_2\}.$$

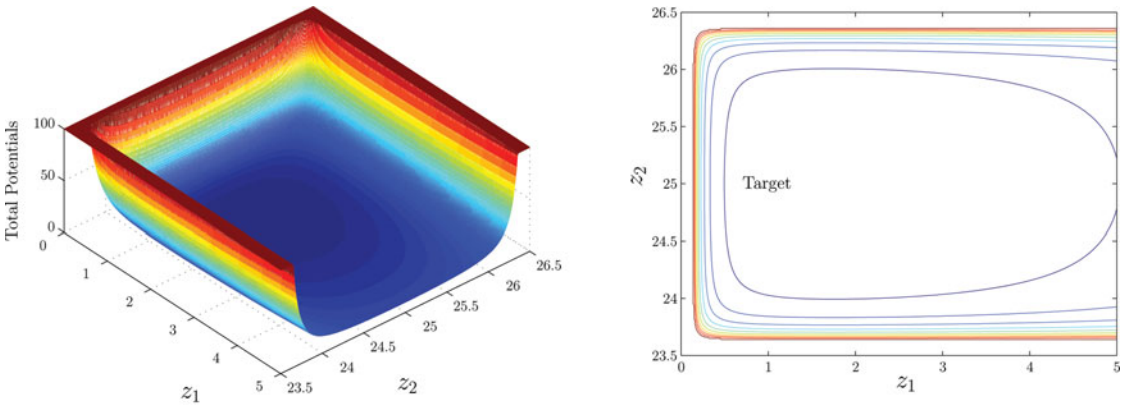

(a) 3D Visualization (b) Contour Plot

Fig. 4. (Colour online) The total potentials generated for target attraction and avoidance of the ghost walls of the parking bay for $\mathcal{A}_1$. The target is located at $(p_{11}, p_{12}) = (1, 25)$. The initial and final coordinates of the three ghost walls are $(A_{11}, B_{11}) = (0, 26.5)$, $(A_{12}, B_{12}) = (0, 23.5)$, $(A_{21}, B_{21}) = (0, 26.5)$, $(A_{22}, B_{22}) = (5, 26.5)$, $(A_{31}, B_{31}) = (0, 23.5)$ and $(A_{32}, B_{32}) = (5, 23.5)$, while $\tau_{1K} = 1$, $K = 1, 2, 3$. (a) 3D visualization. (b) Contour plot.

We require each $\mathcal{A}_i$ to stay within the rectangular region of the WS at all time $t \geq 0$. As such, the boundaries of the WS are considered as fixed obstacles and for their avoidance by each articulated body of $\mathcal{A}_i$, we adopt the following obstacle avoidance functions:

$$W_{i\,4m+1}(\mathbf{x}) := x_{im} - r_m, \qquad W_{i\,4m+2}(\mathbf{x}) := y_{im} - r_m,$$
$$W_{i\,4m+3}(\mathbf{x}) := \eta_1 - (r_m + x_{im}), \quad W_{i\,4m+4}(\mathbf{x}) := \eta_2 - (r_m + y_{im}).$$

It is clear that $W_{i\,4m+1}, W_{i\,4m+3} > 0$ for all $x_{im} \in (r_m, \eta_1 - r_m)$ and $W_{i\,4m+2}, W_{i\,4m+4} > 0$ for all $y_{im} \in (r_m, \eta_2 - r_m)$.

5.2.2. Stationary solid objects. To the authors' knowledge this is the first time that various types of obstacles are treated within the obstacle and collision avoidance scheme of multiple nDNMs.

5.2.3. Category 1: disk-shaped obstacles. Let us fix $q \in \mathbb{N}$ disk-shaped obstacles within the WS. The lth disk-shaped obstacle is defined as a circular disk with center given as (o_{l1}, o_{l2}) and radius rad_l. For avoidance by the mth body of $\mathcal{A}_i$, we consider the obstacle avoidance function

$$FO_{iml}(\mathbf{x}) := \frac{1}{2}\left[(x_{im} - o_{l1})^2 + (y_{im} - o_{l2})^2 - (r_m + rad_l)^2\right],$$

for $l = 1, 2, \ldots, q$.

5.2.4. Category 2: rod-shaped obstacles. Let us fix $z \in \mathbb{N}$ rod-shaped obstacles within the WS. We assume that the $\tilde{k}$th rod-shaped obstacle can be collapsed into a straight line segment with initial coordinates $(a_{\tilde{k}1}, b_{\tilde{k}1})$ and final coordinates $(a_{\tilde{k}2}, b_{\tilde{k}2})$.[5] The parametric representation of the $\tilde{k}$th line segment can be given as

$$c_{im\tilde{k}} := a_{\tilde{k}1} + \lambda_{im\tilde{k}}(a_{\tilde{k}2} - a_{\tilde{k}1}), \qquad d_{im\tilde{k}} := b_{\tilde{k}1} + \lambda_{im\tilde{k}}(b_{\tilde{k}2} - b_{\tilde{k}1}),$$

where $\tilde{k} = 1, 2, \ldots, z$. Using the MDT for the avoidance of these z line segments, we get

$$\lambda_{im\tilde{k}}(x_{im}, y_{im}) := \begin{cases} 0 & , \text{ if } \lambda_{im\tilde{k}} < 0, \\ \lambda_{im\tilde{k}} & , \text{ if } 0 \leq \lambda_{im\tilde{k}} \leq 1, \\ 1 & , \text{ if } \lambda_{im\tilde{k}} > 1, \end{cases}$$

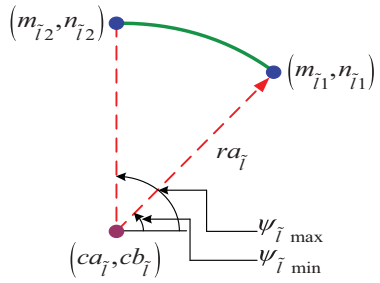

Fig. 5. (Colour online) The $\tilde{l}$th curve-shaped obstacle collapsed into an arc with center $(ca_{\tilde{l}}, cb_{\tilde{l}})$ and radius $ra_{\tilde{l}}$.

with

$$\lambda_{im\tilde{k}} = (x_{im} - a_{\tilde{k}1})q_{\tilde{k}1} + (y_{im} - b_{\tilde{k}1})q_{\tilde{k}2}, \quad \text{for} \quad \lambda_{im\tilde{k}} \in [0, 1],$$

where

$$q_{\tilde{k}1} := \frac{a_{\tilde{k}2} - a_{\tilde{k}1}}{(a_{\tilde{k}2} - a_{\tilde{k}1})^2 + (b_{\tilde{k}2} - b_{\tilde{k}1})^2}, \qquad q_{\tilde{k}2} := \frac{b_{\tilde{k}2} - b_{\tilde{k}1}}{(a_{\tilde{k}2} - a_{\tilde{k}1})^2 + (b_{\tilde{k}2} - b_{\tilde{k}1})^2},$$

which guarantee avoidance of the $\tilde{k}$th rod-shaped fixed obstacle at every iteration $t \geq 0$. For avoidance, we consider the obstacle avoidance function

$$RO_{im\tilde{k}}(\mathbf{x}) := \frac{1}{2}\left[(x_{im} - c_{im\tilde{k}})^2 + (y_{im} - d_{im\tilde{k}})^2 - r_m^2\right], \tag{7}$$

for $\tilde{k} = 1, 2, \ldots, z$.

5.2.5. Category 3: curve-shaped obstacles. Let us fix $\tilde{s} \in \mathbb{N}$ curve-shaped obstacles within the WS. Adopting the nomenclature and methodology of Sharma *et al.* in,[27] we assume that the $\tilde{l}$th curve-shaped obstacle can be collapsed into an arc in the z_1-z_2 plane with initial coordinates $(m_{\tilde{l}1}, n_{\tilde{l}1})$ and final coordinates $(m_{\tilde{l}2}, n_{\tilde{l}2})$, which can be extended from a center $(ca_{\tilde{l}}, cb_{\tilde{l}})$ (see Fig. 5).

The parametric representation of the $\tilde{l}$th arc can be given as $x_{\tilde{l}} := ca_{\tilde{l}} + ra_{\tilde{l}} \cos\psi_{\tilde{l}}$ and $y_{\tilde{l}} := cb_{\tilde{l}} + ra_{\tilde{l}} \sin\psi_{\tilde{l}}$, where $ra_{\tilde{l}}$ is the radius and $\psi_{\tilde{l}} \in [\psi_{\tilde{l}\ \min}, \psi_{\tilde{l}\ \max}]$, with reference to the main-axis.

Again, using the MDT, the coordinates of the point that provides the minimum distance from $\mathcal{A}_i$ can be given as $x_{im\tilde{l}} = ca_{\tilde{l}} + ra_{\tilde{l}} \cos\psi_{im\tilde{l}}$, $y_{im\tilde{l}} = cb_{\tilde{l}} + ra_{\tilde{l}} \sin\psi_{im\tilde{l}}$, where

$$\psi_{im\tilde{l}} := \text{atan2}\,(y_{im} - cb_{\tilde{l}}, x_{im} - ca_{\tilde{l}}),$$

and the modified saturation function $\psi_{im\tilde{l}} \in \mathbb{R}$, adopted from,[27] is

$$\psi_{im\tilde{l}}(x_{im}, y_{im}) := \begin{cases} \psi_{\tilde{l}\ \min}, & \text{if } \psi_{im\tilde{l}} < \psi_{\tilde{l}\ \min}, \\ \psi_{im\tilde{l}}, & \text{if } \psi_{\tilde{l}\ \min} \leq \psi_{im\tilde{l}} \leq \psi_{\tilde{l}\ \max}, \\ \psi_{\tilde{l}\ \max}, & \text{if } \psi_{im\tilde{l}} > \psi_{\tilde{l}\ \max}. \end{cases}$$

Since $\psi_{im\tilde{l}}(x_{im}, y_{im})$ is restricted to the interval $[\psi_{\tilde{l}\ \min}, \psi_{\tilde{l}\ \max}]$, there is always an avoidance of the $\tilde{l}$th curve-shaped fixed obstacle at every iteration $t \geq 0$. For avoidance, we have

$$CO_{im\tilde{l}}(\mathbf{x}) := \frac{1}{2}\left[(x_{im} - x_{im\tilde{l}})^2 + (y_{im} - y_{im\tilde{l}})^2 - r_m^2\right], \tag{8}$$

for $\tilde{l} = 1, 2, \ldots, \tilde{s}$.

Figure 6 presents a 3D view of the total potentials and the corresponding contour plot generated from the attractive function governed by Eq. (5) and the repulsive potential functions designed from Eqs. (7) and (8) for a 3DNM upon treating the velocity and angular components as constants. A

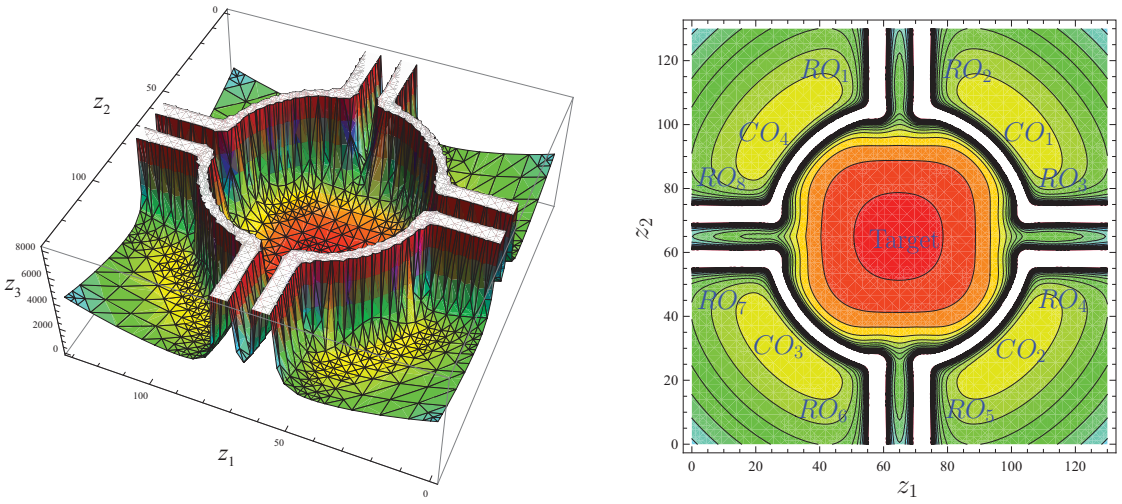

(a) 3D Visualization (b) Contour Plot

Fig. 6. (Colour online) The total potentials (corresponds to the z_3-axis) for target attraction and avoidance of multiple rod-shaped and curve-shaped obstacles by the wheeled platform of a 3DNM with the target fixed at $(p_{11}, p_{12}) = (65, 65)$. Also, $v_1 = 2$, $\omega_{10} = \omega_{11} = \omega_{12} = \pi/360$, $\theta_{10} = 0$, $\theta_{11} = \pi/3$, $\theta_{12} = -\pi/3$, and $\theta_{13} = -\pi/4$. (a) 3D visualization. (b) Contour plot.

roundabout-type obstacle is created with an appropriate combination of rod-shaped and curve-shaped obstacle segments with a global target in the middle.

5.2.6. Moving obstacles. Each solid body of the mobile manipulator has to be treated as a moving obstacle for all the other nDNMs in the WS. Therefore, for each mth component of $\mathcal{A}_i$ to avoid the uth moving solid body of $\mathcal{A}_j$, the avoidance function is

$$MO_{muij}(\mathbf{x}) := \frac{1}{2}\left[(x_{im} - x_{ju})^2 + (y_{im} - y_{ju})^2 - (r_m + r_u)^2\right],$$

for $j = 1, 2, \ldots, N$, $j \neq i$.

5.2.7. Artificial obstacles from dynamic constraints and mechanical singularities. The instantaneous velocities of the mobile platform and the n links of $\mathcal{A}_i$ are restricted due to safety considerations, and the rotation angles of Link k, for $k = 1, 2, \ldots, n$, are restricted due to mechanical singularities. The only way these dynamic constraints can be treated within the framework of the LbCS is to construct an *artificial obstacle* associated to each constraint and then avoid it to solicit the desired restriction.

5.2.8. Category 1: modulus bound on velocities. We limit the translational and the rotational velocities of the nDNMs as follows:[30]

(i) $|v_i| < v_{\max}$, where $v_{\max}$ is the maximal achievable speed;
(ii) $|\omega_{i0}| < v_{\max}/|\rho_{\min}|$, where $\rho_{\min} = \ell_0/\tan(\phi_{\max})$ and $\phi_{\max}$ is maximal steering angle;
(iii) $|\omega_{i1}| < \omega_{1\max}$ and $|\omega_{i2}| < \omega_{2\max}$, where $\omega_{1\max}$ and $\omega_{2\max}$ are the maximal rotational velocities of the first joint and the driving input wheel, respectively.

For simplicity, the values of $v_{\max}$, $\phi_{\max}$, $\omega_{1\max}$, and $\omega_{2\max}$ are kept the same for each $\mathcal{A}_i$.

Next, we model the constraints as artificial obstacles. From (i) above, we define the artificial obstacle

$$AO_{i1} := \{v_i \in \mathbb{R} : v_i \leq -v_{\max} \text{ or } v_i \geq v_{\max}\}.$$

To avoid it, we can use the function

$$U_{i1}(\mathbf{x}) := \frac{1}{2}(v_{\max} - v_i)(v_{\max} + v_i),$$

noting that $U_{i1} > 0$ for $v_i \notin AO_{i1}$, that is, for $-v_{\max} < v_i < v_{\max}$, which is the requirement in (i). Similarly, we can create artificial obstacles from (ii) and (iii) and use similarly defined functions for their avoidance. In summary, our avoidance functions that can ensure that the inequalities in (i)–(iii) are satisfied are:

$$U_{i1}(\mathbf{x}) := \tfrac{1}{2}\,(v_{\max} - v_i)\,(v_{\max} + v_i)\,, \qquad U_{i2}(\mathbf{x}) := \tfrac{1}{2}\left(\tfrac{v_{\max}}{|\rho_{\min}|} - \omega_{i0}\right)\left(\tfrac{v_{\max}}{|\rho_{\min}|} + \omega_{i0}\right),$$

$$U_{i3}(\mathbf{x}) := \tfrac{1}{2}\,(\omega_{1\,\max} - \omega_{i1})\,(\omega_{1\,\max} + \omega_{i1})\,,\; U_{i4}(\mathbf{x}) := \tfrac{1}{2}\,(\omega_{2\,\max} - \omega_{i2})\,(\omega_{2\,\max} + \omega_{i2})\,.$$

5.2.9. Category 2: mechanical singularities. Singular configurations arise from $\mathcal{A}_i$ when $\theta_{im} = 0$, $\theta_{im} = \pi$ or $\theta_{im} = -\pi$, for $m = 2, 3, \ldots, n$, implying that the links can neither be fully stretched nor folded onto each other. The artificial obstacles corresponding to these singularities are

$$AO_{i\;m+3} := \{\theta_{im} \in \mathbb{R} : \theta_{im} = 0, \theta_{im} = \pi \;\text{ or }\; \theta_{im} = -\pi\}.$$

For their avoidance, we consider the functions

$$S_{i\;2m-3}(\mathbf{x}) := |\theta_{im}| \text{ and } S_{i\;2m-2}(\mathbf{x}) := \pi - |\theta_{im}|,$$

for $\theta_{im} \in (-\pi, 0) \cup (0, \pi)$, where $m = 2, 3, \ldots, n$. We also note that the angle between Link 1 and the mobile platform is bounded, that is, Link 1 can freely rotate within $(-\pi/2, \pi/2)$.Therefore, we have

$$S_{i\;2n-1}(\mathbf{x}) := \frac{1}{2}\left(\frac{\pi}{2} - \theta_{i1}\right)\left(\frac{\pi}{2} + \theta_{i1}\right),$$

for the avoidance of the artificial obstacle

$$AO_{i\;n+4} := \{\theta_{i1} \in \mathbb{R} : \theta_{i1} \le -\pi/2 \;\text{ or }\; \theta_{i1} \ge \pi/2\}.$$

5.3. Auxiliary function

To ensure that the total potentials vanish at the target configuration, we use an auxiliary function

$$F_i(\mathbf{x}) := \frac{1}{2}\left[(x_i - p_{i1})^2 + (y_i - p_{i2})^2 + \rho_{i0}(\theta_{i0} - p_{i3})^2 + \sum_{k=1}^{n} \rho_{ik}(\theta_{ik} - p_{i\;k+3})^2\right]. \tag{9}$$

Note that p_{i3} and $p_{i\;k+3}$ are the desired final orientations of the platform and Link k, respectively. Here, ρ_{i0} and ρ_{ik} are new parameters classified as the *angle-gain parameters*, which will be used to force prescribed final orientations of each solid body of $\mathcal{A}_i$. An angle-gain parameter will have a value of 1 if a final orientation is prescribed; else it gets a default value of 0.

6. Controllers and Stability Analysis

The nonlinear control laws for our dynamic system (1) will be designed using the Lyapunov-based control scheme, which will also provide a mathematical proof of stability of system (3) via the Direct Method of Lyapunov.

6.1. Lyapunov function

We now construct the total potentials, that is, a Lyapunov function for system (3). First, we introduce the following parameters that we will use in the repulsive potential functions:

(i) $\tau_{iK} > 0$, $K = 3i - 2, 3i - 1, 3i$, for the avoidance of the walls of the ghost parking bays (see Subsection 5.1);

(ii) $\alpha_{is} > 0$, $s = 1, \ldots, 4n+4$, for the avoidance of the boundaries of the workspace WS (see Subsection 5.2.1);
(iii) $\gamma_{iml} > 0, l = 1, \ldots, q$, for the avoidance of q disk-shaped obstacles (see Subsection 5.2.2);
(iv) $\psi_{im\tilde{k}} > 0, \tilde{k} = 1, \ldots, z$, for the avoidance of z rod-shaped obstacles (see Subsection 5.2.2);
(v) $\kappa_{im\tilde{l}} > 0, \tilde{l} = 1, \ldots, \tilde{s}$, for the avoidance of $\tilde{s}$ curve-shaped obstacles (see Subsection 5.2.2);
(vi) $\zeta_{muij} > 0$, $j \neq i$, for the collision avoidance between any two nDNMs (see Subsection 5.2.6);
(vii) $\beta_{ir} > 0$, $r = 1, \ldots, 4$, and $\xi_{ip} > 0$, $p = 1, \ldots, 2n-1$, for the avoidance of the artificial obstacles from dynamic constraints (see Subsection 5.2.7).

These are basically *tuning* or *control parameters*. Using these, we now propose the following Lyapunov function for system (3) with two components, namely, the attractive and repulsive potential field components:

$$V(\mathbf{x}) := \sum_{i=1}^{N} \left\{ H_i(\mathbf{x}) + F_i(\mathbf{x}) \left[\sum_{s=1}^{4n+4} \frac{\alpha_{is}}{W_{is}(\mathbf{x})} + \sum_{r=1}^{4} \frac{\beta_{ir}}{U_{ir}(\mathbf{x})} + \sum_{p=1}^{2n-1} \frac{\xi_{ip}}{S_{ip}(\mathbf{x})} + \sum_{K=3i-2}^{3i} \frac{\tau_{iK}}{PB_{iK}(\mathbf{x})} \right] \right.$$
$$+ F_i(\mathbf{x}) \sum_{m=0}^{n} \left(\sum_{l=1}^{q} \frac{\gamma_{iml}}{FO_{iml}(\mathbf{x})} + \sum_{\tilde{k}=1}^{z} \frac{\psi_{im\tilde{k}}}{RO_{im\tilde{k}}(\mathbf{x})} + \sum_{\tilde{l}=1}^{\tilde{s}} \frac{\kappa_{im\tilde{l}}}{CO_{im\tilde{l}}(\mathbf{x})} \right)$$
$$\left. + F_i(\mathbf{x}) \sum_{\substack{j=1 \\ j \neq i}}^{N} \sum_{m=0}^{n} \sum_{u=0}^{n} \frac{\zeta_{muij}}{MO_{muij}(\mathbf{x})} \right\}.$$

The tentative Lyapunov function is locally positive definite and continuous over the domain

$$D(V) := \{ \mathbf{x} \in \mathbb{R}^{(n+7)\times N} : W_{is}(\mathbf{x}) > 0, s = 1, \ldots, 4n+4; \;\; U_{ir}(\mathbf{x}) > 0, r = 1, \ldots, 4;$$
$$MO_{muij}(\mathbf{x}) > 0, j = 1, \ldots, N, j \neq i; \;\; S_{ip}(\mathbf{x}) > 0, p = 1, \ldots, 2n-1;$$
$$FO_{iml}(\mathbf{x}) > 0, l = 1, \ldots, q; \;\; RO_{im\tilde{k}}(\mathbf{x}) > 0, \tilde{k} = 1, \ldots, z;$$
$$CO_{im\tilde{l}}(\mathbf{x}) > 0, \tilde{l} = 1, \ldots, \tilde{s}; \;\; PB_{imK}(\mathbf{x}) > 0, K = 3i-2, 3i-1, 3i \}.$$

Indeed, $V(\mathbf{x}^*) = 0$ since $H_i(\mathbf{x}_i^*) = 0$ and $F_i(\mathbf{x}_i^*) = 0$. Hence, $\mathbf{x}^* \in D(V)$ and is an equilibrium point of system (3).

We shall show at the end of this section that $D(V)$ is a positively invariant set, meaning that if $\mathbf{x}(0) \in D(V)$, then $\mathbf{x}(t) \in D(V)$ for all $t \geq 0$. The implication of this is that V guarantees the avoidance of every type of obstacle.

6.2. Nonlinear acceleration controllers

The process of designing the feedback controllers begins by finding the time-derivative of V along every solution of system (3) and forcing it to be at least negative semi-definite on $D(V)$. After a tedious but straightforward derivation, it can be shown that

$$\dot{V}_{(3)}(\mathbf{x}) = \sum_{i=1}^{N} \left[f_{i1}(\mathbf{x}) \dot{x}_i + f_{i2}(\mathbf{x}) \dot{y}_i + \sum_{m=0}^{n} \left(f_{i\,2m+3}(\mathbf{x}) \dot{x}_{im} + f_{i\,2m+4}(\mathbf{x}) \dot{y}_{im} + g_{i\,m+1}(\mathbf{x}) \dot{\theta}_{im} \right) \right]$$
$$+ \sum_{i=1}^{N} \left[g_{i\,n+1}(\mathbf{x}) v_i \dot{v}_i + \sum_{j=0}^{2} g_{i\,n+(j+3)}(\mathbf{x}) \omega_{ij} \dot{\omega}_{ij} \right],$$

where, for the sake of brevity, we have collected all the attraction and collision avoidance functions appropriately in the functions f_{i1}, f_{i2}, $f_{i\,2m+3}$, $f_{i\,2m+4}$, $g_{i\,m+1}$, $g_{i\,n+1}$ and $g_{i\,n+(j+3)}$, which are listed in the Appendix. We can further simplify $\dot{V}_{(3)}(\mathbf{x})$ by collecting terms with each velocity, v_i, ω_{i0}, ω_{i1}

or ω_{i2}; that is,

$$\dot{V}_{(3)}(\mathbf{x}) = \sum_{i=1}^{N} \left[G_{i1}(\mathbf{x}) v_i + G_{i2}(\mathbf{x}) \omega_{i0} + G_{i3}(\mathbf{x}) \omega_{i1} + G_{i4}(\mathbf{x}) \omega_{i2} \right],$$

where G_{i1}, G_{i2}, G_{i3} and G_{i4} are also listed in the Appendix. Then, keeping in mind that $\dot{v}_i = u_{i1}$, $\dot{\omega}_{i0} = u_{i2}$, $\dot{\omega}_{i1} = u_{i3}$ and $\dot{\omega}_{i2} = u_{i4}$, it is a simple matter to show that for some scalars $\delta_{ij} > 0$, for $j = 1, \ldots, 4$ and $i = 1, \ldots, N$, we have

$$\dot{V}_{(3)}(\mathbf{x}) = -\sum_{i=1}^{N} \left(\delta_{i1} v_i^2 + \sum_{j=0}^{2} \delta_{i\ j+2} \omega_{ij}^2 \right) \leq 0,$$

provided the accelerations are defined as

$$\left.\begin{aligned} u_{i1} &= -\left(\delta_{i1} v_i + G_{i1}\right) / g_{i\ n+1}, \quad u_{i2} = -\left(\delta_{i2} \omega_{i0} + G_{i2}\right) / g_{i\ n+2}, \\ u_{i3} &= -\left(\delta_{i3} \omega_{i1} + G_{i3}\right) / g_{i\ n+3}, \quad u_{i4} = -\left(\delta_{i4} \omega_{i2} + G_{i4}\right) / g_{i\ n+4}. \end{aligned}\right\} \tag{10}$$

We note that the Direct Method of Lyapunov produces feedback controllers, which therefore depend explicitly on the state variables, $\mathbf{x} = \mathbf{x}(t)$ and hence implicitly on time, t. That is, $u_{i1}(t) = u_{i1}(\mathbf{x}(t))$, $u_{i2}(t) = u_{i2}(\mathbf{x}(t))$, $u_{i3}(t) = u_{i3}(\mathbf{x}(t))$ and $u_{i4}(t) = u_{i4}(\mathbf{x}(t))$.

Via these controllers every $\mathcal{A}_i$ has the information on the positions of all other $\mathcal{A}_j$ and its own target, without a need for a centralized entity to provide the information. Hence, the controllers are classified as decentralized.

6.3. Stability analysis

It is clear that $\dot{V}_{(3)}(\mathbf{x}) \leq 0$ for all $\mathbf{x} \in D(V)$. Moreover, it is easily seen that $\dot{V}_{(3)}(\mathbf{x}^*) = 0$. We have thus just proven that V is indeed a Lyapunov function for system (3) whose equilibrium point $\mathbf{x}^*$ is stable in the Lyapunov sense.

We summarize our findings in the following theorem, wherein $\mathbf{h}(\mathbf{x}) := \mathbf{f}(\mathbf{x}) + \mathbf{B}\mathbf{u}(\mathbf{x})$.

Theorem 1. Let u_{i1}, u_{i2}, u_{i3} and u_{i4}, for all $i = 1, \ldots, N$, be as defined in (10) for system (3). Then $\mathbf{h} \in C^1[D(V), \mathbb{R}^{(n+7)\times N}]$ and for every initial condition $\mathbf{x}_0 \in D(V)$, system (3) has a stable equilibrium point $\mathbf{x}^* \in D(V)$.

Proof. We have

$$g_{i\ n+1} = 1 + F_i \frac{\beta_{i1}}{U_{i1}^2}, \quad g_{i\ n+2} = 1 + F_i \frac{\beta_{i2}}{U_{i2}^2}, \quad g_{i\ n+3} = 1 + F_i \frac{\beta_{i3}}{U_{i3}^2}, \quad g_{i\ n+4} = 1 + F_i \frac{\beta_{i4}}{U_{i4}^2}.$$

Since U_{i1}, U_{i2}, U_{i3} and U_{i4} appear in the denominator, they will also appear in the denominator of higher order partial derivatives of $g_{i\ n+1}$, $g_{i\ n+2}$, $g_{i\ n+3}$ and $g_{i\ n+4}$, and hence in the higher order partial derivatives of u_{i1}, u_{i2}, u_{i3} and u_{i4}, respectively, with respect to the variables in $\mathbf{x}$. Similarly, all the avoidance functions listed in $D(V)$ and that are in the denominator of the terms in G_{i1}, G_{i2}, G_{i3} and G_{i4} will also appear in the denominator of the terms in the higher order partial derivatives of u_{i1}, u_{i2}, u_{i3} and u_{i4}, respectively. Hence, the higher order partial derivatives of u_{i1}, u_{i2}, u_{i3} and u_{i4} are also continuous on $D(V)$. Since the other ODEs in (1) also have higher order partial derivatives in $\mathbf{x}$, with each continuous over $D(V)$, we have that $\mathbf{h} \in C^1[D(V), \mathbb{R}^{(n+7)\times N}]$; that is, $\mathbf{h}$ is locally Lipschitz on $D(V)$. This implies there are unique solutions of system (3) in $D(V)$. To prove their stability, it is easy to see that $V(\mathbf{x}) > 0$ for all $\mathbf{x} \in D(V)/\mathbf{x}^*$, $V(\mathbf{x}^*) = 0$, $\dot{V}_{(3)}(\mathbf{x}) \leq 0$ for all $\mathbf{x} \in D(V)$, and $\dot{V}_{(3)}(\mathbf{x}^*) = 0$. Hence, it is clear that $V \in C^1[D(V), \mathbb{R}_+]$, where $\mathbb{R}_+ = [0, +\infty)$, and is indeed a Lyapunov function for system (3). Thus, the conclusion of Theorem 1 readily follows from the Direct Method of Lyapunov. □

Corollary 1. *Every solution* $\mathbf{x} \in D(V)$ *of system (3) converges to the largest invariant set contained in* $S_0 := \{\mathbf{x} \in D(V) : \dot{V}(\mathbf{x}) = 0\}$.

Proof. By Theorem 1, all solutions of system (3) in $D(V)$ are bounded. Hence the convergence to the largest invariant set in S_0 is guaranteed by LaSalle's Invariance Principle. □

The fact that $\mathbf{x}(t) \to S_0$ as $t \to \infty$ shows that a trajectory of system (3), with an appropriate initial condition, could approach a neighborhood of $\mathbf{x}^* \in S_0$. This does not contradict Brockett's result on nonholonomic systems[31] because it is clear that the largest invariant set in S_0 does not contain only $\mathbf{x}^*$.

6.4. Guarantee of obstacle avoidance

The fact that $\mathbf{h}$ is continuously differentiable on $D(V)$ implies that $D(V)$ is a positively invariant set, meaning that if $\mathbf{x}(0) \in D(V)$, then $\mathbf{x}(t) \in D(V)$ for all $t \geq 0$. This, in turn, implies that the avoidance of every type of obstacle, physical or artificial, is guaranteed via the Lyapunov function V. To prove that $D(V)$ is a positively invariant set, we simply invoke the existence, uniqueness and continuity of the solutions of (3) in a standard argument expounded in Khalil,[32] page 653.

Corollary 2. *The set* $D(V)$ *is positively invariant.*

Proof. The existence of solutions in $D(V)$ (as guaranteed by Theorem 1) allows us to let, say, $\chi(t; \mathbf{y}) \in D(V)$ be the solution of (3) that passes through a point $\mathbf{y} \in D(V)$ at $t = 0$; that is, $\chi(0; \mathbf{y}) = \mathbf{y} \in D(V)$. In other words, for a solution $\mathbf{x}(t) \in D(V)$, there must be a sequence $\{t_k\}$ with $t_k \to \infty$ such that $\mathbf{x}(t_k) \to \mathbf{y}$ as $k \to \infty$. One then has that $\mathbf{x}(t_k) = \chi(t_k; \mathbf{x}_0)$, where $\mathbf{x}_0$ is the initial state of $\mathbf{x}(t)$ at $t = 0$.

By the uniqueness of solutions,

$$\chi(t + t_k; \mathbf{x}_0) = \chi(t; \chi(t; \mathbf{x}_0)) = \chi(t; \mathbf{x}(t_k))$$

where, for sufficiently large k, $t + t_k > 0$.

By the continuity of solutions,

$$\lim_{t\to\infty} \chi(t + t_k; \mathbf{x}_0) = \lim_{t\to\infty} \chi(t; \mathbf{x}(t_k)) = \chi(t; \mathbf{y})$$

which shows that

$$\chi(0; \mathbf{y}) \in D(V) \Rightarrow \chi(t; \mathbf{y}) \in D(V) \ \ \forall t \geq 0, \ \ \forall \mathbf{y} \in D(V).$$

□

7. Simulations

This section demonstrates the computer simulation results from two interesting traffic situations, for the 3-link doubly nonholonomic mobile manipulators (3DNMs) navigating in a constrained workspace cluttered with obstacles. In both scenarios we assume that the dimensions of the mobile manipulators are the same. The effectiveness of the LbCS and the resulting decentralized acceleration controllers will be verified numerically.

7.1. Scenario 1

This scenario will consider eight 3DNMs in a virtual traffic roundabout situation, each entering from one highway and then navigating into a prescribed highway while adhering to the right-hand rule pertaining to the traffic situations and attaining a prescribed final posture. Moreover, the 3DNMs will have to avoid multiple moving and stationary obstacles intercepting their paths, and the obstacle spaces generated by the artificial obstacles created for the dynamic constraints tagged to the robotic systems. In addition to generating final prescribed final orientations of the eight 3DNMs, we have utilized these walls and strategically placed rod-shaped obstacles to form the boundaries of the

Table II. *Scenario 1.* Initial and final states of eight 3DNMs.

$\mathcal{A}_i$	(x_i, y_i)	$(\theta_{i0}, \theta_{i1}, \theta_{i2}, \theta_{i3})$	$(p_{i1}, p_{i2}, p_{i3}, p_{i4}, p_{i5}, p_{i6})$
$\mathcal{A}_1$	(69, 20)	$\left(-\frac{\pi}{2}, \frac{\pi}{3}, -\frac{\pi}{4}, -\frac{\pi}{4}\right)$	$\left(69, 15, -\frac{\pi}{2}, \frac{\pi}{3}, -\frac{\pi}{4}, -\frac{\pi}{4}\right)$
$\mathcal{A}_2$	(69, 105)	$\left(-\frac{\pi}{2}, \frac{\pi}{3}, -\frac{\pi}{4}, -\frac{\pi}{4}\right)$	$\left(128, 69, 0, \frac{\pi}{3}, -\frac{\pi}{4}, -\frac{\pi}{4}\right)$
$\mathcal{A}_3$	(120, 61)	$\left(\pi, \frac{\pi}{3}, -\frac{\pi}{4}, -\frac{\pi}{4}\right)$	$\left(15, 61, \pi, \frac{\pi}{3}, -\frac{\pi}{4}, -\frac{\pi}{4}\right)$
$\mathcal{A}_4$	(105, 61)	$\left(\pi, \frac{\pi}{3}, -\frac{\pi}{4}, -\frac{\pi}{4}\right)$	$\left(69, 2, -\frac{\pi}{2}, \frac{\pi}{3}, -\frac{\pi}{4}, -\frac{\pi}{4}\right)$
$\mathcal{A}_5$	(61, 10)	$\left(\frac{\pi}{2}, \frac{\pi}{3}, -\frac{\pi}{4}, -\frac{\pi}{4}\right)$	$\left(61, 115, \frac{\pi}{2}, \frac{\pi}{3}, -\frac{\pi}{4}, -\frac{\pi}{4}\right)$
$\mathcal{A}_6$	(61, 25)	$\left(\frac{\pi}{2}, \frac{\pi}{3}, -\frac{\pi}{4}, -\frac{\pi}{4}\right)$	$\left(2, 61, \pi, \frac{\pi}{3}, -\frac{\pi}{4}, -\frac{\pi}{4}\right)$
$\mathcal{A}_7$	(10, 69)	$\left(0, \frac{\pi}{3}, -\frac{\pi}{4}, -\frac{\pi}{4}\right)$	$\left(115, 69, -\frac{\pi}{2}, \frac{\pi}{3}, -\frac{\pi}{4}, -\frac{\pi}{4}\right)$
$\mathcal{A}_8$	(25, 69)	$\left(0, \frac{\pi}{3}, -\frac{\pi}{4}, -\frac{\pi}{4}\right)$	$\left(61, 128, \frac{\pi}{2}, \frac{\pi}{3}, -\frac{\pi}{4}, -\frac{\pi}{4}\right)$

Table III. *Scenario 2.* Initial and final states of five 3DNMs.

$\mathcal{A}_i$	(x_i, y_i)	$(\theta_{i0}, \theta_{i1}, \theta_{i2}, \theta_{i3})$	$(p_{i1}, p_{i2}, p_{i3}, p_{i4}, p_{i5}, p_{i6})$
$\mathcal{A}_1$	(5, 7)	$\left(\frac{\pi}{4}, \frac{\pi}{3}, -\frac{\pi}{4}, -\frac{\pi}{4}\right)$	$\left(47.5, 49.5, \frac{\pi}{4}, \frac{\pi}{3}, -\frac{\pi}{4}, -\frac{\pi}{4}\right)$
$\mathcal{A}_2$	(8, 43)	$\left(-\frac{\pi}{4}, \frac{\pi}{3}, -\frac{\pi}{4}, -\frac{\pi}{4}\right)$	$\left(48, 0.5, -\frac{\pi}{4}, \frac{\pi}{3}, -\frac{\pi}{4}, -\frac{\pi}{4}\right)$
$\mathcal{A}_3$	(45, 25)	$\left(\pi, \frac{\pi}{3}, -\frac{\pi}{4}, -\frac{\pi}{4}\right)$	$\left(1, 25, \pi, \frac{\pi}{3}, -\frac{\pi}{4}, -\frac{\pi}{4}\right)$
$\mathcal{A}_4$	(40, 7)	$\left(\frac{3\pi}{4}, \frac{\pi}{3}, -\frac{\pi}{4}, -\frac{\pi}{4}\right)$	$\left(2.5, 48.5, \pi, \frac{\pi}{3}, -\frac{\pi}{4}, -\frac{\pi}{4}\right)$
$\mathcal{A}_5$	(25, 5)	$\left(\frac{\pi}{2}, \frac{\pi}{3}, -\frac{\pi}{4}, -\frac{\pi}{4}\right)$	$\left(25, 49, \frac{\pi}{2}, \frac{\pi}{3}, -\frac{\pi}{4}, -\frac{\pi}{4}\right)$

highways and create dual-lanes, namely, left and right lanes. The corresponding initial and final states of the eight 3DNMs are provided in Table II. For this scenario, $i = 1, 2, \ldots, 8$ and $m = 0, 1, 2, 3$.

Figure 7 shows the paths taken by the eight 3DNMs and their convergence to the desired goals. In the final phase, the wheeled platform and each of the three links of the manipulator system achieved a pre-determined final orientation with the aid of the ghost parking bays and the new attractive auxiliary function given by Eq. (9). As an illustration, we have provided the orientations of the articulated bodies of $\mathcal{A}_1$, see Fig. 8(a). One can notice that there was a convergence to the target with θ_{10}, θ_{11}, θ_{12}, and θ_{13}, in a small neighborhood of the prescribed final orientations.

To illustrate the convergent property of the control laws, graphs of the acceleration components of $\mathcal{A}_1$ (shown in Fig. 8(b)) have been generated. The corresponding graphs of the remaining 3DNMs will show similar convergent properties along the system trajectories.

For the four curve-shaped obstacles $(ca_{\tilde{l}}, cb_{\tilde{l}}) = (65, 65)$ and $ra_{\tilde{l}} = 40$, for $\tilde{l} = 1, \ldots, 4$, with $\psi_{1\,\min} = 0.18$, $\psi_{1\,\max} = 1.39$, $\psi_{2\,\min} = -1.39$, $\psi_{2\,\max} = -0.18$, $\psi_{3\,\min} = -2.97$, $\psi_{3\,\max} = -1.75$, $\psi_{4\,\min} = 1.75$, and $\psi_{4\,\max} = 2.97$.

The numerical values of the control parameters are as follows:

(i) $\tau_{imK} = 0.001$, $K = 1, 2, 3, 4$;
(ii) $\alpha_{is} = 0.1$, $s = 1, \ldots, 16$;
(iii) $\gamma_{im1} = 10$;
(iv) $\psi_{im\tilde{k}} = 0.1$, $\tilde{k} = 1, \ldots, 8$;
(v) $\kappa_{im\tilde{l}} = 0.1$, $\tilde{l} = 1, \ldots, 4$;
(vi) $\zeta_{muij} = 0.0001$, $u = 0, \ldots, 3$, $j = 1, \ldots, 8$, $j \neq i$;
(vi) $\beta_{ir} = 2$, $r = 1, \ldots, 4$, and $\xi_{ip} = 0.0001$, $p = 1, \ldots, 5$.

7.2. Scenario 2

This scenario considers five 3DNMs ($i = 1, 2, \ldots, 5$ and $m = 0, 1, 2, 3$) and depicts a virtual scenario that shows the three possible types of parking: row, diagonal, and parallel. The corresponding initial and final states of the five 3DNMs are provided in Table III.

The dimensions of the five 3DNMs are $\ell_0 = 4$, $b_0 = 2$ and $\ell_1 = \ell_2 = \ell_3 = 2$.

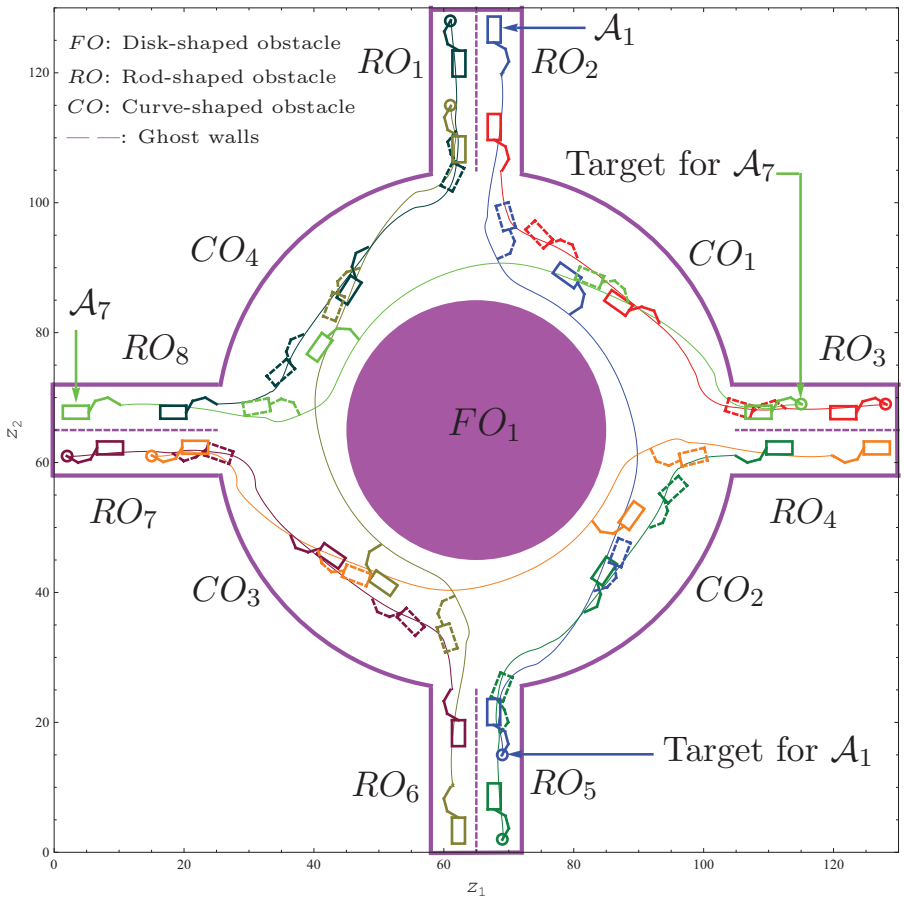

Fig. 7. (Colour online) *Scenario 1.* The resulting trajectories of the 3DNMs with dimensions $\ell_0 = 1.5$, $b_0 = 0.7$ and $\ell_1 = \ell_2 = \ell_3 = 0.7$. Also, $\rho_{i0} = 1$, $\rho_{ik} = 1$ ($k = 1, 2, 3$), $\delta_{ij} = 200$, $j = 1, \ldots, 4$, the initial velocities are $v_i(0) = 3$, $\omega_{i0}(0) = 0.2$, and $\omega_{i1}(0) = \omega_{i2}(0) = 0.05$, for $i = 1, \ldots, 8$.

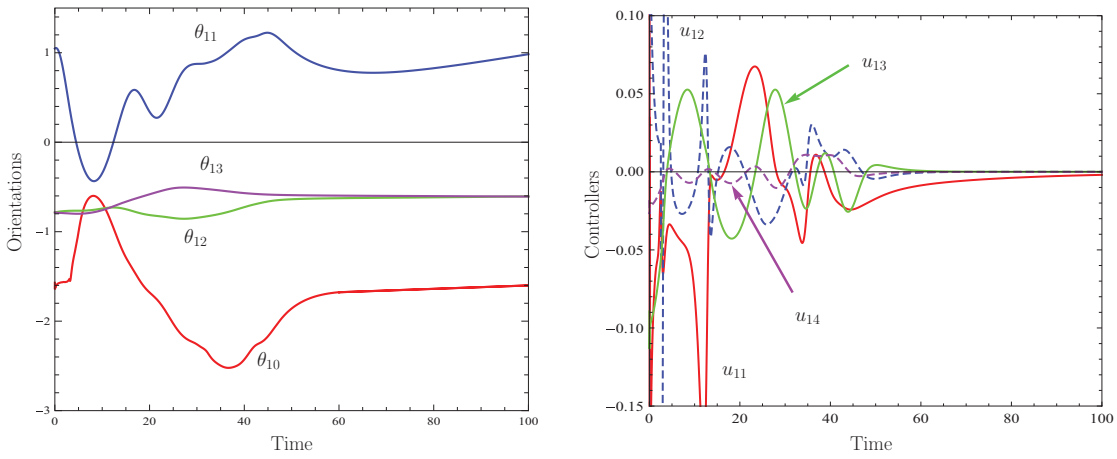

(a) Orientations of $\mathcal{A}_1$. (b) Controllers of $\mathcal{A}_1$.

Fig. 8. (Colour online) *Scenario 1.* (a) portrays the evolution of the orientations of the various bodies of $\mathcal{A}_1$, while (b) depicts the evolution of its decentralized acceleration controls. (a) Orientations of $\mathcal{A}_1$. (b) Controllers of $\mathcal{A}_1$.

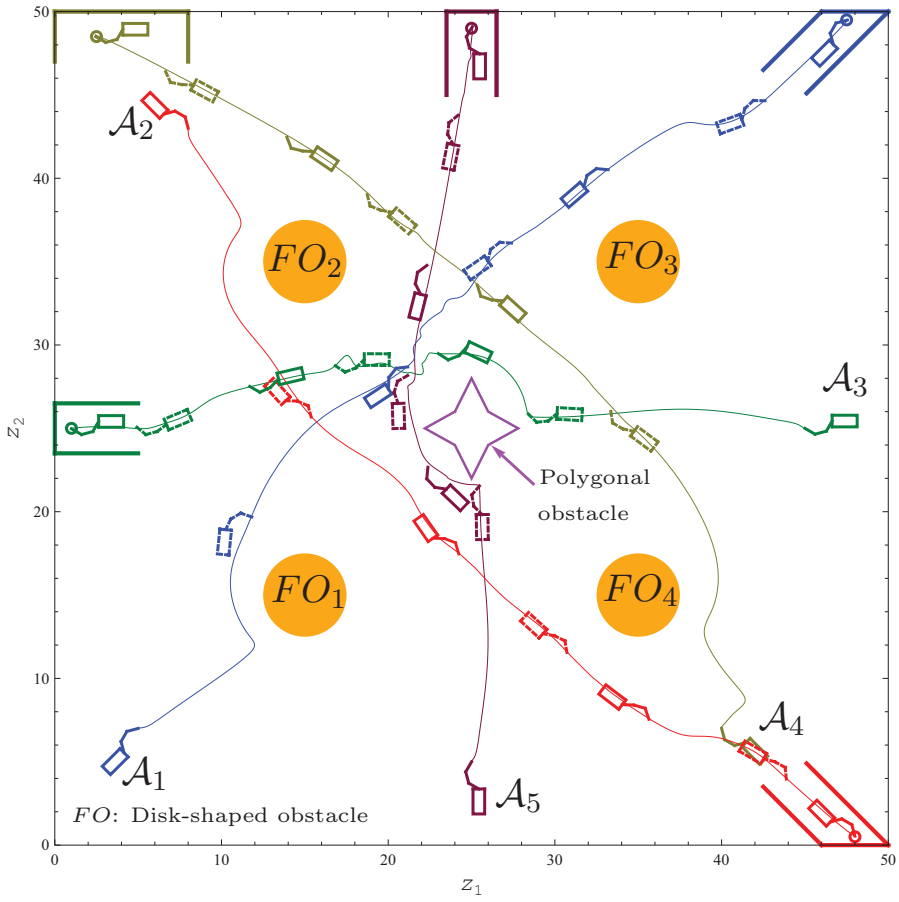

Fig. 9. (Colour online) *Scenario 2*. The resulting trajectories of the 3DNMs with angle-gain parameters, $\rho_{i0} = 1$, $\rho_{ik} = 1, k = 1, 2, 3$ and convergence parameters $\delta_{ij} = 550$, $j = 1, \ldots, 4$.

The numerical values of the control parameters are as follows:

(i) $\tau_{imK} = 0.001$, $K = 1, \ldots, 15$;
(ii) $\alpha_{is} = 0.1$, $s = 1, \ldots, 16$;
(iii) $\gamma_{iml} = 0.5$, $l = 1, \ldots, 4$;
(iv) $\psi_{im\tilde{k}} = 0.1$, $\tilde{k} = 1, \ldots, 8$;
(v) $\kappa_{im\tilde{l}} = 0$;
(vi) $\zeta_{muij} = 0.01$, $u = 0, \ldots, 3$, $j = 1, \ldots, 5$, $j \neq i$;
(vi) $\beta_{ir} = 2$, $r = 1, \ldots, 4$, and $\xi_{ip} = 0.0001$, $p = 1, \ldots, 5$.

Figure 9 shows the paths taken by the five 3DNMs and their convergence to the desired goals with the deployment of the proposed acceleration controllers and appropriate values of the various parameters. With reference to Fig. 9, we have incorporated a polygonal (star-shaped) fixed obstacle within the WS, which is made up of rod-shaped obstacles. An avoidance scheme for each segment was considered together with the avoidance of the fixed and moving obstacles in the workspace. One can clearly notice that the 3DNMs successfully avoided fixed and moving obstacles in their paths while traversing to their final goals.

We have provided the orientations of the platforms of the mobile manipulators, see Fig. 10(a). This shows that the ghost parking bays ensured that the 3DNMs achieved their predefined orientations at their desired goals.

To illustrate the convergent property of the control laws, graph of the acceleration components of $\mathcal{A}_2$ (shown in Fig. 10(b)) has been generated. The initial large values have been truncated for a

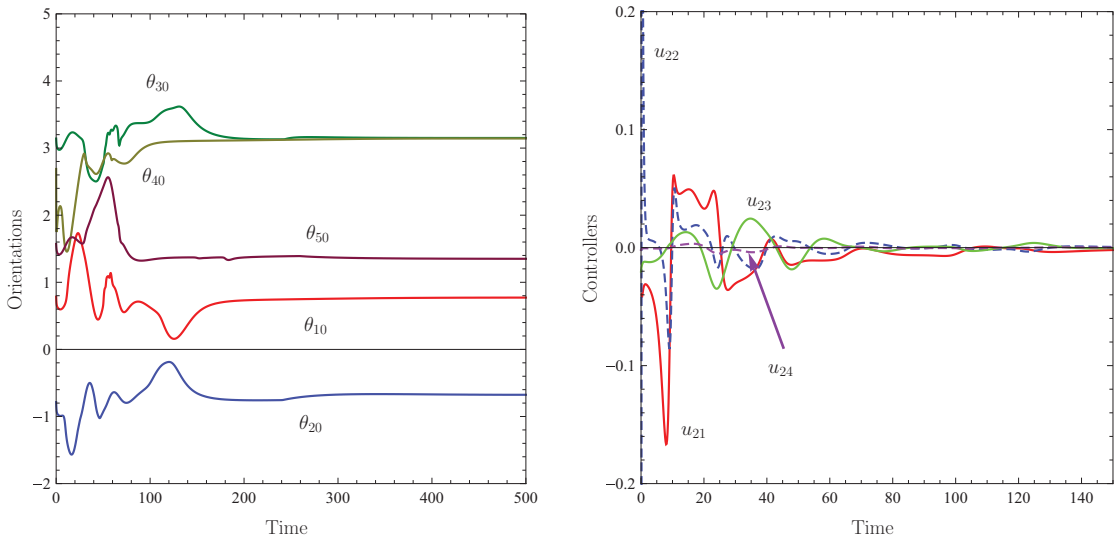

(a) Orientations. (b) Controllers of $\mathcal{A}_2$.

Fig. 10. (Colour online) *Scenario 2.* (a) shows the evolution of the orientations of the wheeled platforms of the 3DNMs while (b) depicts the progression of the acceleration controllers of $\mathcal{A}_2$. (a) Orientations. (b) Controllers of $\mathcal{A}_2$.

better visualization of the evolution of the controllers. The convergence is easily observed after the avoidance of the obstacles. The corresponding graphs of the remaining mobile manipulators will show similar convergent properties along the system trajectories.

8. Conclusion and Future Work

Ultimately, the design of a decentralized motion and control planner for multi-tasking of multi-vehicle systems is a complex, computer intensive yet interesting problem. In this paper, we have presented decentralized continuous acceleration control laws that have successfully guided multiple doubly nonholonomic mobile manipulators to their respective targets in the presence of fixed, moving and artificial obstacles in a constrained and bounded environment. The concepts of minimum distance technique and ghost parking bays were also utilized to attain final postures of the multi-agents. Synthesis of these nonlinear controllers was via the Lyapunov-based control scheme. To the authors' knowledge, this was the first time decentralized continuous controls have been designed for motion planning and posture control of multiple n-link doubly nonholonomic mobile manipulators. In addition, this approach intrinsically guaranteed the stability of the robotic system. The effectiveness of the proposed control laws was demonstrated via successful computer simulations.

Future work includes motion planning and posture control of a team of n-link doubly nonholonomic mobile manipulators fixed at various degrees of the formation stiffness to carry out specific real-world tasks and applications.

Acknowledgment

The authors would like to thank the referees and Professor Jun-Hong Ha, of Korea University of Technology and Education, for their comments which have led to an improvement in content and presentation.

References

1. W. Burgard, M. Moors, C. Stachniss and F. E. Schneider, "Coordinated multi-robot exploration," *IEEE Trans. Robot.* **21**(3), 376–386 (2005).
2. J. L. Fuller, *Introduction, Programming, and Projects* (Prentice Hall, 1998).

3. H. Hu, P. W. Tsui, L. Cragg and N. Völker, "Architecture for multi-robot cooperation over the internet," *Int. J. Integr. Comput.-Aided Eng.* **11**(3), 213–226 (2004).
4. B. Sharma, J. Vanualailai and A. Prasad, "Formation control of a swarm of mobile manipulators," *Rocky Mt. J. Math.* **41**(3), 900–940 (2011).
5. B. Sharma, New Directions in the Applications of the Lyapunov-based Control Scheme to the Findpath Problem *Ph.D. Thesis* (University of the South Pacific, Suva, Fiji Islands, July 2008). PhD Dissertation.
6. H. Yamaguchi, "A distributed motion coordination strategy for multiple nonholonomic mobile robots in cooperative hunting operations," *Robot. Auton. Syst.* **43**(4), 257–282 (2003).
7. B. Sharma, J. Vanualailai and A. Prasad, "Trajectory planning and posture control of multiple mobile manipulators," *Int. J. Appl. Math. Comput.* **2**(1), 11–31 (2010).
8. A. Campbell and S. W. Annie, "Learning and Exploiting Knowledge in Multi-Agent Task Allocation Problems," *Proceedings of the Evolutionary Computation and Multi-Agent Systems and Simulation (ECoMASS) Workshop*, London, England (July 7–11, 2007) pp. 2637–2642.
9. H. Seraji, "A unified approach to motion control of mobile manipulators," *Int. J. Robot. Res.* **17**(2), 107–118 (1998).
10. J. Tan and N. Xi, "Unified Model Approach for Planning and Control for Mobile Manipulators," *Proceedings of the 2001 IEEE International Conference on Robotics and Automation*, Seoul, Korea (May, 2001) pp. 3145–3152.
11. A. Mazur and K. Arent, "Trajectory Tracking Control for Nonholonomic Mobile Manipulators," **In:** *Robot Motion and Control* (K. Kozlouski, ed.) (Springer-Verlag, 2006) pp. 55–71.
12. A. Mazur and D. Szakiel, "On path following control of nonholonomic mobile manipulators," *Int. J. Appl. Math. Comput. Sci.* **19**(4), 561–574 (2009).
13. H. Su and V. Krovi, "Decentralized Dynamic Control of a Nonholonomic Mobile Manipulator Collective: A Simulation Study," *Proceedings of the 2008 ASME Dynamic Systems and Control Conference*, Michigan, USA (Oct. 2008) pp. 1–8.
14. K. Tchoń, J. Jakubiak and K. Zadarnowska, "Doubly Nonholonomic Mobile Manipulators," *Proceedings IEEE International Conference on Robotics and Automation*, New Orleans (2004) pp. 4590–4595.
15. A. D. Chohra, F. Sif and S. Talaoubrid, "Neural Navigation Approach of an Autonomous Mobile Robot in a Partially Structured Environment," *Proceedings of IAV'95*, Finland (Jun. 1995) pp. 238–243.
16. D. Janglova, "Neural networks in mobile robot motion," *Int. J. Adv. Robot. Syst.* **1**(1) 15–22 (2004).
17. J. M. Skowronski, *Nonlinear Lyapunov Dynamics* (World Scientific Publishers, 1990).
18. J. Vanualailai, B. Sharma and S. Nakagiri, "An asymptotically stable collision-avoidance system," *Int. J. Non-Linear Mech.* **43**(9) 925–932 (2008).
19. S. X. Yang and M. Meng, "An efficient neural network approach to dynamic robot motion planning," *Neural Netw.* **13**(2), 143–148 (2000).
20. L. Edelstein-Keshet, "Mathematical Models of Swarming and Social Aggregation," *Proceedings of 2001 International Symposium on Nonlinear Theory and its Applications*, Miyagi, Japan (Oct.–Nov. 2001) pp. 1–7.
21. H. Ouarda, "Neural path planning for mobile robots," *Int. J. Syst. Appl. Eng. Dev.* **5**(3), 367–376 (1997).
22. O. Khatib, "Real time obstacle avoidance for manipulators and mobile robots," *Int. J. Robot. Res.* **7**(1), 90–98 (1986).
23. L-F. Lee and V. Krovi, "A Standardized Testing-Ground for Artificial Potential-Field based Motion Planning for Robot Collectives," *Proceedings of the Performance Metrics for Intelligent Systems Workshop*, Gaithersburg (Aug. 2006).
24. Y. S. Nam, B. H. Lee and N. Y. Ko, "An Analytic Approach to Moving Obstacle Avoidance using Anartificial Potential Field," *Proceedings of IEEE/RSJ International Conference on Intelligent Robots and Systems*, vol. 2 (Aug. 1995) pp. 482–487.
25. P. Song and V. Kumar, "A Potential Field based Approach to Multi-Robot Manipulation," *Proceedings of the IEEE International Conference on Robotics & Automation*, Washington, DC (May 2002).
26. B. Sharma, J. Vanualailai and U. Chand, "Flocking of multi-agents in constrained environments," *Eur. J. Pure Appl. Math.* **2**(3), 401–425 (2009).
27. B. Sharma, J. Vanualailai and S. Singh, "Tunnel passing maneuvers of prescribed formations," *Int. J. Robust Nonlinear Control* **24**(5), 876–901 (2014).
28. B. Sharma, J. Vanualailai and S. Singh, "Lyapunov-based nonlinear controllers for obstacle avoidance with a planar n-link doubly nonholonomic manipulator," *Robot. Auton. Syst.* **60**, 1484–1497 (2012). `http://dx.doi.org/10.1016/j.bbr.2011.03.031`,.
29. Y. Nakamura, W. Chung and O. J. Sørdalen, "Design and control of the nonholonomic manipulator," *IEEE Trans. Robot. Autom.* **17**(1), 48–59 (2003).
30. G. J. Pappas and K. J. Kyriakopoulos, "Stabilization of non-holonomic vehicle under kinematic constraints," *Int. J. Control* **61**(4), 933–947 (1995).
31. R. W. Brockett, "Asymptotic Stability and Feedback Stabilisation," **In:** *Differential Geometry Control Theory* (Springer-Verlag, 1983) pp. 181–191.
32. H. K. Khalil, *Nonlinear Systems*, 2nd ed. (Prentice-Hall, New Jersey, 1996).

Appendix

On suppressing **x**, we define, for $i = 1, 2, \ldots, N$ and $m = 1, 2, \ldots, n$,

$$f_{i1} := \left[1 + \sum_{s=1}^{4n+4} \frac{\alpha_{is}}{W_{is}} + \sum_{r=1}^{4} \frac{\beta_{ir}}{U_{ir}} + \sum_{p=1}^{2n-1} \frac{\xi_{ip}}{S_{ip}} + \sum_{\substack{j=1 \\ j\neq i}}^{N} \sum_{m=0}^{n} \sum_{u=0}^{n} \frac{\zeta_{muij}}{MO_{muij}}\right](x_i - p_{i1})$$
$$+ \left[\sum_{m=0}^{n} \left(\sum_{l=1}^{q} \frac{\gamma_{iml}}{FO_{iml}} + \sum_{\tilde{k}=1}^{z} \frac{\psi_{im\tilde{k}}}{RO_{im\tilde{k}}} + \sum_{\tilde{l}=1}^{\tilde{s}} \frac{\kappa_{im\tilde{l}}}{CO_{im\tilde{l}}}\right) + \sum_{K=3i-2}^{3i} \frac{\tau_{iK}}{PB_{iK}}\right](x_i - p_{i1}),$$

$$f_{i2} := \left[1 + \sum_{s=1}^{4n+4} \frac{\alpha_{is}}{W_{is}} + \sum_{r=1}^{4} \frac{\beta_{ir}}{U_{ir}} + \sum_{p=1}^{2n-1} \frac{\xi_{ip}}{S_{ip}} + \sum_{\substack{j=1 \\ j\neq i}}^{N} \sum_{m=0}^{n} \sum_{u=0}^{n} \frac{\zeta_{muij}}{MO_{muij}}\right](y_i - p_{i2})$$
$$+ \left[\sum_{m=0}^{n} \left(\sum_{l=1}^{q} \frac{\gamma_{iml}}{FO_{iml}} + \sum_{\tilde{k}=1}^{z} \frac{\psi_{im\tilde{k}}}{RO_{im\tilde{k}}} + \sum_{\tilde{l}=1}^{\tilde{s}} \frac{\kappa_{im\tilde{l}}}{CO_{im\tilde{l}}}\right) + \sum_{K=3i-2}^{3i} \frac{\tau_{iK}}{PB_{iK}}\right](y_i - p_{i2}),$$

$$f_{i3} := -F_i \left[\frac{\alpha_{i1}}{W_{i1}^2} - \frac{\alpha_{i3}}{W_{i3}^2} + \sum_{l=1}^{q} \frac{\gamma_{i0l}}{FO_{i0l}^2}(x_{i0} - o_{l1})\right]$$
$$-F_i \sum_{\tilde{k}=1}^{z} \frac{\psi_{i0\tilde{k}}}{RO_{i0\tilde{k}}^2} \left[(x_{i0} - c_{i0\tilde{k}})\left[1 - (a_{\tilde{k}2} - a_{\tilde{k}1})q_{\tilde{k}1}\right] - (y_{i0} - d_{i0\tilde{k}})(b_{\tilde{k}2} - b_{\tilde{k}1})q_{\tilde{k}1}\right]$$
$$-F_i \sum_{\tilde{l}=1}^{\tilde{s}} \frac{\kappa_{i0\tilde{l}}}{CO_{i0\tilde{l}}^2} \left[1 - ra_{\tilde{l}} \frac{(y_{i0} - cb_{\tilde{l}})\sin\psi_{i0\tilde{l}}}{(x_{i0} - ca_{\tilde{l}})^2 + (y_{i0} - cb_{\tilde{l}})^2}\right](x_{i0} - x_{i0\tilde{l}})$$
$$-F_i \sum_{\tilde{l}=1}^{\tilde{s}} \frac{\kappa_{i0\tilde{l}}}{CO_{i0\tilde{l}}^2} \left[ra_{\tilde{l}} \frac{(y_{i0} - cb_{\tilde{l}})\cos\psi_{i0\tilde{l}}}{(x_{i0} - ca_{\tilde{l}})^2 + (y_{i0} - cb_{\tilde{l}})^2}\right](y_{i0} - y_{i0\tilde{l}})$$
$$-F_i \sum_{K=3i-2}^{3i} \frac{\tau_{iK}}{PB_{iK}^2}(x_{i0} - C_{iK})\left[1 - (A_{K2} - A_{K1})Q_{K1}\right]$$
$$+F_i \sum_{K=3i-2}^{3i} \frac{\tau_{iK}}{PB_{iK}^2}(y_{i0} - D_{iK})(B_{K2} - B_{K1})Q_{K1}$$
$$+\sum_{\substack{j=1 \\ j\neq i}}^{N} \sum_{u=0}^{n} \left[F_j \frac{\zeta_{u0ji}}{MO_{u0ji}^2}(x_{ju} - x_{i0}) - F_i \frac{\zeta_{0uij}}{MO_{0uij}^2}(x_{i0} - x_{ju})\right],$$

$$f_{i4} := -F_i \left[\frac{\alpha_{i2}}{W_{i2}^2} - \frac{\alpha_{i4}}{W_{i4}^2} + \sum_{l=1}^{q} \frac{\gamma_{i0l}}{FO_{i0l}^2}(y_{i0} - o_{l2})\right]$$
$$-F_i \sum_{\tilde{k}=1}^{z} \frac{\psi_{i0\tilde{k}}}{RO_{i0\tilde{k}}^2} \left[(y_{i0} - d_{i0\tilde{k}})\left[1 - (b_{\tilde{k}2} - b_{\tilde{k}1})q_{\tilde{k}2}\right] - (x_{i0} - c_{i0\tilde{k}})(a_{\tilde{k}2} - a_{\tilde{k}1})q_{\tilde{k}2}\right]$$

$$-F_i \sum_{\tilde{l}=1}^{\tilde{s}} \frac{\kappa_{i0\tilde{l}}}{CO_{i0\tilde{l}}^2} \left[1 - ra_{\tilde{l}} \frac{(x_{i0} - ca_{\tilde{l}})\cos\psi_{i0\tilde{l}}}{(x_{i0} - ca_{\tilde{l}})^2 + (y_{i0} - cb_{\tilde{l}})^2}\right](y_{i0} - y_{i0\tilde{l}})$$

$$-F_i \sum_{\tilde{l}=1}^{\tilde{s}} \frac{\kappa_{i0\tilde{l}}}{CO_{i0\tilde{l}}^2} \left[ra_{\tilde{l}} \frac{(x_{i0} - ca_{\tilde{l}})\sin\psi_{i0\tilde{l}}}{(x_{i0} - ca_{\tilde{l}})^2 + (y_{i0} - cb_{\tilde{l}})^2}\right](x_{i0} - x_{i0\tilde{l}})$$

$$-F_i \sum_{K=3i-2}^{3i} \frac{\tau_{iK}}{PB_{iK}^2}(y_{i0} - D_{iK})\left[1 - (B_{K2} - B_{K1})Q_{K2}\right]$$

$$+F_i \sum_{K=3i-2}^{3i} \frac{\tau_{iK}}{PB_{iK}^2}(x_{i0} - C_{iK})(A_{K2} - A_{K1})Q_{K2}$$

$$+\sum_{\substack{j=1\\ j\neq i}}^{N}\sum_{u=0}^{n}\left[F_j \frac{\zeta_{u0ji}}{MO_{u0ji}^2}(y_{ju} - y_{i0}) - F_i \frac{\zeta_{0uij}}{MO_{0uij}^2}(y_{i0} - y_{ju})\right],$$

$$f_{i\ 2m+3} := -F_i\left[\frac{\alpha_{i\ 4m+1}}{W_{i\ 4m+1}^2} - \frac{\alpha_{i\ 4m+3}}{W_{i\ 4m+3}^2} + \sum_{l=1}^{q} \frac{\gamma_{iml}}{FO_{iml}^2}(x_{im} - o_{l1})\right]$$

$$-F_i \sum_{\tilde{k}=1}^{z} \frac{\psi_{im\tilde{k}}}{RO_{im\tilde{k}}^2}\left[(x_{im} - c_{im\tilde{k}})\left[1 - (a_{\tilde{k}2} - a_{\tilde{k}1})q_{\tilde{k}1}\right] - (y_{im} - d_{im\tilde{k}})(b_{\tilde{k}2} - b_{\tilde{k}1})q_{\tilde{k}1}\right]$$

$$-F_i \sum_{\tilde{l}=1}^{\tilde{s}} \frac{\kappa_{im\tilde{l}}}{CO_{im\tilde{l}}^2}\left[1 - ra_{\tilde{l}} \frac{(y_{im} - cb_{\tilde{l}})\sin\psi_{im\tilde{l}}}{(x_{im} - ca_{\tilde{l}})^2 + (y_{im} - cb_{\tilde{l}})^2}\right](x_{im} - x_{im\tilde{l}})$$

$$-F_i \sum_{\tilde{l}=1}^{\tilde{s}} \frac{\kappa_{im\tilde{l}}}{CO_{im\tilde{l}}^2}\left[ra_{\tilde{l}} \frac{(y_{im} - cb_{\tilde{l}})\cos\psi_{im\tilde{l}}}{(x_{im} - ca_{\tilde{l}})^2 + (y_{im} - cb_{\tilde{l}})^2}\right](y_{im} - y_{im\tilde{l}})$$

$$+\sum_{\substack{j=1\\ j\neq i}}^{N}\sum_{u=0}^{n}\left[F_j \frac{\zeta_{umji}}{MO_{umji}^2}(x_{ju} - x_{im}) - F_i \frac{\zeta_{muij}}{MO_{muij}^2}(x_{im} - x_{ju})\right],$$

$$f_{i\ 2m+4} := -F_i\left[\frac{\alpha_{i\ 4m+2}}{W_{i\ 4m+2}^2} - \frac{\alpha_{i\ 4m+4}}{W_{i\ 4m+4}^2} + \sum_{l=1}^{q} \frac{\gamma_{iml}}{FO_{iml}^2}(y_{im} - o_{l2})\right]$$

$$-F_i \sum_{\tilde{k}=1}^{z} \frac{\psi_{im\tilde{k}}}{RO_{im\tilde{k}}^2}\left[(y_{im} - d_{im\tilde{k}})\left[1 - (b_{\tilde{k}2} - b_{\tilde{k}1})q_{\tilde{k}2}\right] - (x_{im} - c_{im\tilde{k}})(a_{\tilde{k}2} - a_{\tilde{k}1})q_{\tilde{k}2}\right]$$

$$-F_i \sum_{\tilde{l}=1}^{\tilde{s}} \frac{\kappa_{im\tilde{l}}}{CO_{im\tilde{l}}^2}\left[1 - ra_{\tilde{l}} \frac{(x_{im} - ca_{\tilde{l}})\cos\psi_{im\tilde{l}}}{(x_{im} - ca_{\tilde{l}})^2 + (y_{im} - cb_{\tilde{l}})^2}\right](y_{im} - y_{im\tilde{l}})$$

$$-F_i \sum_{\tilde{l}=1}^{\tilde{s}} \frac{\kappa_{im\tilde{l}}}{CO_{im\tilde{l}}^2}\left[ra_{\tilde{l}} \frac{(x_{im} - ca_{\tilde{l}})\sin\psi_{im\tilde{l}}}{(x_{im} - ca_{\tilde{l}})^2 + (y_{im} - cb_{\tilde{l}})^2}\right](x_{im} - x_{im\tilde{l}})$$

$$+\sum_{\substack{j=1\\ j\neq i}}^{N}\sum_{u=0}^{n}\left[F_j \frac{\zeta_{umji}}{MO_{umji}^2}(y_{ju} - y_{im}) - F_i \frac{\zeta_{muij}}{MO_{muij}^2}(y_{im} - y_{ju})\right],$$

$$g_{i1} := \left[\sum_{s=1}^{4n+4}\frac{\alpha_{is}}{W_{is}} + \sum_{r=1}^{4}\frac{\beta_{ir}}{U_{ir}} + \sum_{p=1}^{2n-1}\frac{\xi_{ip}}{S_{ip}} + \sum_{\substack{j=1\\ j\neq i}}^{N}\sum_{m=0}^{n}\sum_{u=0}^{n}\frac{\zeta_{muij}}{MO_{muij}}\right](\theta_{i0} - p_{i3})$$
$$+\left[\sum_{m=0}^{n}\left(\sum_{l=1}^{q}\frac{\gamma_{iml}}{FO_{iml}} + \sum_{\tilde{k}=1}^{z}\frac{\psi_{im\tilde{k}}}{RO_{im\tilde{k}}} + \sum_{\tilde{l}=1}^{\tilde{s}}\frac{\kappa_{im\tilde{l}}}{CO_{im\tilde{l}}}\right) + \sum_{K=3i-2}^{3i}\frac{\tau_{imK}}{PB_{imK}}\right](\theta_{i0} - p_{i3}),$$

$$g_{i2} := \left[\sum_{s=1}^{4n+4}\frac{\alpha_{is}}{W_{is}} + \sum_{r=1}^{4}\frac{\beta_{ir}}{U_{ir}} + \sum_{p=1}^{2n-1}\frac{\xi_{ip}}{S_{ip}} + \sum_{\substack{j=1\\ j\neq i}}^{N}\sum_{m=0}^{n}\sum_{u=0}^{n}\frac{\zeta_{muij}}{MO_{muij}}\right](\theta_{i1} - p_{i4})$$
$$+\sum_{m=0}^{n}\left(\sum_{l=1}^{q}\frac{\gamma_{iml}}{FO_{iml}} + \sum_{\tilde{k}=1}^{z}\frac{\psi_{im\tilde{k}}}{RO_{im\tilde{k}}} + \sum_{\tilde{l}=1}^{\tilde{s}}\frac{\kappa_{im\tilde{l}}}{CO_{im\tilde{l}}}\right)(\theta_{i1} - p_{i4}),$$

$$g_{i\,n+1} := 1 + F_i\frac{\beta_{i1}}{U_{i1}^2}, \quad g_{i\,n+2} := 1 + F_i\frac{\beta_{i2}}{U_{i2}^2}, \quad g_{i\,n+3} := 1 + F_i\frac{\beta_{i3}}{U_{i3}^2}, \quad g_{i\,n+4} := 1 + F_i\frac{\beta_{i4}}{U_{i4}^2}.$$

For $m = 2, 3, \ldots, n$

$$g_{i\,m+1} := \left[\sum_{s=1}^{4n+4}\frac{\alpha_{is}}{W_{is}} + \sum_{r=1}^{4}\frac{\beta_{ir}}{U_{ir}} + \sum_{p=1}^{2n-1}\frac{\xi_{ip}}{S_{ip}} + \sum_{\substack{j=1\\ j\neq i}}^{N}\sum_{m=0}^{n}\sum_{u=0}^{n}\frac{\zeta_{muij}}{MO_{muij}}\right](\theta_{im} - p_{i\,m+3})$$
$$+\sum_{m=0}^{n}\left(\sum_{l=1}^{q}\frac{\gamma_{iml}}{FO_{iml}} + \sum_{\tilde{k}=1}^{z}\frac{\psi_{im\tilde{k}}}{RO_{im\tilde{k}}} + \sum_{\tilde{l}=1}^{\tilde{s}}\frac{\kappa_{im\tilde{l}}}{CO_{im\tilde{l}}} + \sum_{K=3i-2}^{3i}\frac{\tau_{imK}}{PB_{imK}}\right)(\theta_{im} - p_{i\,m+3})$$
$$-F_i\left(\frac{\xi_{i\,2m-3}}{S_{i\,2m-3}^2} - \frac{\xi_{i\,2m-2}}{S_{i\,2m-2}^2}\right)\frac{|\theta_{im}|}{\theta_{im}}.$$

Finally, for the sake of brevity, we let $\mathrm{C}(\cdot) := \cos(\cdot)$, $\mathrm{S}(\cdot) := \sin(\cdot)$, $\theta_{iT} := \theta_{i0} + \theta_{i1}$, and

$$L(m,k) := \frac{\ell_k}{2^{\lfloor\frac{m+1}{k+1}\rfloor}},$$

and define, for $i = 1, 2, \ldots, N$,

$$G_{i1} := \left(f_{i1} + \sum_{m=0}^{n} f_{i\,2m+3}\right)\mathrm{C}(\theta_{i0}) + \left(f_{i2} + \sum_{m=0}^{n} f_{i\,2m+4}\right)\mathrm{S}(\theta_{i0}),$$

$$G_{i2} := -\left(f_{i1} + \sum_{m=0}^{n} f_{i\,2m+3}\right)\left[\ell_0\mathrm{S}(\theta_{i0}) + \sum_{k=1}^{n}\ell_k\mathrm{S}\left(\sum_{p=0}^{k}\theta_{ip}\right)\right]$$
$$+\left(f_{i2} + \sum_{m=0}^{n} f_{i\,2m+4}\right)\left[\ell_0\mathrm{C}(\theta_{i0}) + \sum_{k=1}^{n}\ell_k\mathrm{C}\left(\sum_{p=0}^{k}\theta_{ip}\right)\right]$$
$$+f_{i3}\left(\frac{\ell_0}{2}\mathrm{S}(\theta_{i0}) + \ell_1\mathrm{S}(\theta_{iT})\right) + \frac{\ell_1}{2}f_{i5}\mathrm{S}(\theta_{iT}) - f_{i4}\left(\frac{\ell_0}{2}\mathrm{C}(\theta_{i0}) - \ell_1\mathrm{C}(\theta_{iT})\right) - \frac{\ell_1}{2}f_{i6}\mathrm{C}(\theta_{iT})$$
$$+\sum_{m=2}^{n} f_{i\,2m+3}\left[\sum_{k=m}^{n}L(m,k)\mathrm{S}\left(\sum_{p=0}^{k}\theta_{ip}\right)\right] - \sum_{m=2}^{n} f_{i\,2m+4}\left[\sum_{k=m}^{n}L(m,k)\mathrm{C}\left(\sum_{p=0}^{k}\theta_{ip}\right)\right],$$

$$G_{i3} := -\left(f_{i1} + \sum_{m=0}^{n} f_{i\,2m+3}\right)\sum_{k=1}^{n}\ell_k \mathrm{S}\left(\sum_{p=0}^{k}\theta_{ip}\right) + \left(f_{i2} + \sum_{m=0}^{n} f_{i\,2m+4}\right)\sum_{k=1}^{n}\ell_k \mathrm{C}\left(\sum_{p=0}^{k}\theta_{ip}\right)$$
$$+ f_{i3}\left[\ell_1 \mathrm{S}(\theta_{iT}) + \sum_{k=2}^{n} L(m,k)\mathrm{S}\left(\sum_{p=0}^{k}\theta_{ip}\right)\right] + f_{i5}\left[\frac{\ell_1}{2}\mathrm{S}(\theta_{iT}) + \sum_{k=2}^{n} L(m,k)\mathrm{S}\left(\sum_{p=0}^{k}\theta_{ip}\right)\right]$$
$$- f_{i4}\left[\ell_1 \mathrm{C}(\theta_{iT}) + \sum_{k=2}^{n} L(m,k)\mathrm{C}\left(\sum_{p=0}^{k}\theta_{ip}\right)\right] - f_{i6}\left[\frac{\ell_1}{2}\mathrm{C}(\theta_{iT}) + \sum_{k=2}^{n} L(m,k)\mathrm{C}\left(\sum_{p=0}^{k}\theta_{ip}\right)\right]$$
$$+ \sum_{m=2}^{n} f_{i\,2m+3}\left[\sum_{k=m}^{n} L(m,k)\mathrm{S}\left(\sum_{p=0}^{k}\theta_{ip}\right)\right] - \sum_{m=2}^{n} f_{i\,2m+4}\left[\sum_{k=m}^{n} L(m,k)\mathrm{C}\left(\sum_{p=0}^{k}\theta_{ip}\right)\right] + g_{i1},$$

$$G_{i4} := -\left(f_{i1} + \sum_{m=0}^{n} f_{i\,2m+3}\right)\sum_{k=2}^{n}\ell_k\left(\sum_{p=2}^{k} a_{ip}\mathrm{S}(\theta_{i\,p-1})\prod_{j=1}^{p-2}\mathrm{C}(\theta_{ij})\right)\mathrm{S}\left(\sum_{p=0}^{k}\theta_{ip}\right)$$
$$+ \left(f_{i2} + \sum_{m=0}^{n} f_{i\,2m+4}\right)\sum_{k=2}^{n}\ell_k\left(\sum_{p=2}^{k} a_{ip}\mathrm{S}(\theta_{i\,p-1})\prod_{j=1}^{p-2}\mathrm{C}(\theta_{ij})\right)\mathrm{C}\left(\sum_{p=0}^{k}\theta_{ip}\right)$$
$$+ \sum_{m=0}^{n} f_{i\,2m+3}\left\{\sum_{k=2}^{n} L(m,k)\mathrm{S}\left(\sum_{p=0}^{k}\theta_{ip}\right)\left[\sum_{p=2}^{k}\left(a_{ip}\mathrm{S}(\theta_{i\,p-1})\prod_{j=1}^{p-2}\mathrm{C}(\theta_{ij})\right)\right]\right\}$$
$$- \sum_{m=0}^{n} f_{i\,2m+4}\left\{\sum_{k=2}^{n} L(m,k)\mathrm{C}\left(\sum_{p=0}^{k}\theta_{ip}\right)\left[\sum_{p=2}^{k}\left(a_{ip}\mathrm{S}(\theta_{i\,p-1})\prod_{j=1}^{p-2}\mathrm{C}(\theta_{ij})\right)\right]\right\}$$
$$+ \sum_{m=2}^{n} g_{im}a_{im}\mathrm{S}(\theta_{i\,m-1})\prod_{j=1}^{m-2}\mathrm{C}(\theta_{ij}).$$